Cellular and Molecular Life Sciences (2025) 82:123
https://doi.org/10.1007/s00018-025-05639-3

ORIGINAL ARTICLE

Estrogen-induced circFAM171A1 regulates sheep myoblast proliferation through the oar-miR-485-5p/MAPK15/MAPK pathway

Runqing Chi[1] · Yufang Liu[1,2] · Peng Wang[1] · Fan Yang[1] · Xiangyu Wang[1] · Xiaoyun He[1] · Ran Di[1] · Mingxing Chu[1]

Received: 1 August 2024 / Revised: 19 February 2025 / Accepted: 24 February 2025

Abstract

Estrogen is an important hormone that affects muscle development in female animals. Previous studies have shown that estrogen can protect muscle cells from apoptosis by inhibiting the MAPK signaling pathway. However, the molecular mechanisms by which estrogen-induced MAPK signaling regulates myoblast growth and development remain unclear. In this study, RNA-seq was performed on ovariectomized small-tailed Han (OR-STH) sheep and sham surgery small-tailed Han (STH) sheep to analyze the effects of estrogen on muscle growth and development in female animals. There were 8721 differentially expressed circRNAs (DECs), 143 differentially expressed miRNAs (DEMs) and 2238 differentially expressed mRNAs (DEGs) in the *longissimus dorsi* between the OR-STH and STH groups. Bioinformatics analysis revealed that the differentially expressed gene MAPK15 was significantly enriched in the MAPK signaling pathway, which is important for muscle development. Therefore, we constructed the ceRNA network circFAM171A1/oar-miR-485-5p/MAPK15 and explored its effect on muscle growth and development. The results of the molecular mechanism experiments indicated that circFAM171A1 can sponge oar-miR-485-5p to regulate *MAPK15*. The addition of the exogenous hormone estradiol (E_2) to sheep myoblasts could induce circFAM171A1, regulate the expression of oar-miR-485-5p and *MAPK15*, and promote the proliferation of sheep myoblasts. The results showed that *MAPK15* and circFAM171A1 significantly promoted the proliferation of myoblasts and inhibited the apoptosis of myoblasts in sheep, whereas oar-miR-485-5p inhibited the expression of *MAPK15* and circFAM171A1, inhibited myoblast proliferation and promoted apoptosis. Furthermore, circFAM171A1 attenuated the inhibitory effect of oar-miR-485-5p on myoblasts. In summary, estrogen induced the expression of circFAM171A1 in sheep myoblasts, and circFAM171A1 can act as a sponge for oar-miR-485-5p to promote the expression of the target gene *MAPK15* and ultimately regulate the proliferation of sheep myoblasts. This study provides new insights into the molecular mechanism of estrogen regulation of muscle growth and development in female animals.

Keywords Sheep · Muscle development · Estrogen · Induced circRNA · Oar-miR-485-5p · MAPK15

Introduction

Estrogen is an important hormone that affects muscle development in female animals. It is mainly secreted by the ovary. Previous research suggests that a lack of estrogen induces bone muscle cell apoptosis, leading to a loss of bone muscle quality and force [1]. Studies on mouse C2C12 (myoblast) cells have shown that estrogen exposure can protect against hydrogen peroxide-induced apoptosis by upregulating HSP27, which combines with Caspase-3, blocking its cleavage and inactivating the inhibitor, thereby modulating the downstream targets of Bcl-2, BAD, AKT, ERK, and MAPK and ultimately preventing apoptosis and promoting the viability of C2C12 cells [2–8]. Studies in rodents have shown that estrogen treatment reduces locomotion-induced HSP70

Runqing Chi and Yufang Liu contributed equally.

✉ Ran Di
diran@caas.cn

✉ Mingxing Chu
mxchu@263.net

[1] Present Address: State Key Laboratory of Animal Biotech Breeding, Institute of Animal Science, Chinese Academy of Agricultural Sciences (CAAS), No. 2 Yuanmingyuan West Rd, Beijing 100193, China

[2] Present Address: Anhui Provincial Key Laboratory of Livestock and Poultry Product Safety Engineering, Hefei 230031, China

Published online: 19 March 2025

and HSP72 responses in males or ovariectomized females but has no effect on HSP27 in stifle muscles [9–12]. Wang also revealed that the underlying protein levels of HSP70, HSP27, and HSP90 in bone muscle were reduced in female rats after the loss of estrogen [13]. In addition, Karvinen et al. reported that estrogen resistance downregulates a variety of miRNAs that may inhibit the apoptotic pathway, thus leading to increased cell death and a decrease in bone muscle quality [14]. However, the detailed molecular mechanisms of estrogen in muscle development remain unclear.

Estrogen may play a biological role by inducing the production of circRNAs. In studies of ER-positive breast cancer, estrogen has been found to induce the production of circPGR, which is positioned in the stroma of the cell and serves as a competitive endogenous RNA (ceRNA) to sponge miR-301a-5p, regulating the development of a number of cell cycle factors [15], indicating a mechanism of action by which estrogen functions in animals. CircRNAs in animals are produced by the cyclization of specific exons [16] or a few introns [17], and they are particularly stable RNAs. In vivo, circRNA is produced from the spliceosome by reverse splicing: the 3′ side of the exon is attached by covalent splicing to the 5′ side of the upstream exon and is immune to the nucleic acid epimerase RNase R. The circRNA is also resistant to the nucleic acid epimerase RNase R [18–20]. CircRNAs play a critical role in the development of animal muscle, not only through competitive endogenous RNA to regulate the expression of miRNAs but also through binding to proteins to constitute functional units that are involved in the modulation of biological functions [21]. For example, circHIPK3 can promote skeletal muscle development in chicken embryos by sponging miR-30a-3p [22]. CircRNA FUT10 targets HOXA9 by combining with miR-365a-3p to ameliorate degenerative muscle disorders [23]. CircNDST1 regulates bovine myogenic cell multiplication and specialization through the miR-411a/Smad4 axis [24]. CircFoxo3 delays cell cytosolic advancement by entering into a triplet complex with p21 and CDK2 [25]. Therefore, the above studies suggest that estrogen can first induce specific circRNAs and that these circRNAs can regulate the miRNA-gene pathway to participate in muscle development.

Most of these circRNAs have been characterized in human, mouse, bovine, and porcine myoblasts. The expression of circRNAs throughout in vitro myoblast differentiation in mouse and human cells has been analyzed, and conserved circRNAs have been identified across species during the process of myogenesis and the development of Duchenne dystrophy [26]. Wei et al. obtained circRNA profiles of bovine skeletal muscle at two stages of development (embryonic and mature muscle), revealing for the first time their participation in bovine muscle formation [27]. Sun et al. demonstrated that a number of circRNAs are involved in muscle growth in the *longissimus dorsi* muscles of Rand and Blue Pond pigs [28]. Studies have also identified circRNAs in sheep muscle but have not yet described differences in the expression and action of circRNAs in the muscles of ovariectomized and intact sheep.

Skeletal muscle derives and originates from myogenic progenitor cells (MPCs), which mainly include somatic and myogenic cell multiplication and polarization, myotube fusion, and myofibril formation [29, 30]. Myogenesis is regulated by myogenic factors, including the Pax families Pax3 and Pax7 [31] and the MRF families (Myf5, MyoD, MyoG, and MRF4) [32]. Pax3 is required for the migration of MPCs and, together with a family of MRFs, for mediating myoblast differentiation. Pax3 activates Myf5, which, together with MRF4, affects the process of myoblast proliferation and differentiation. Pax3 is also required for the migration of MPCs and, together with a family of MRFs, for the mediation of myoblast differentiation. [33, 34]. P-CaMK-II promotes myogenic differentiation and the formation of type II myofibers by inhibiting β-catenin and p-ERK1/2 dephosphorylation via activation of the Zac1/GPR39 system [31]. Muscle MSCs also give rise to muscle stem cells (also called satellite cells) that are activated immediately after muscle damage and split into proliferating myoblasts, which are characterized by the presence of Pax7 and MyoD [35, 36]. Although the transcriptional regulation of myogenesis has been explored, the essential functions of noncoding RNAs (e.g., circRNAs and miRNAs) during myogenesis are worthy of further investigation.

The objective of this study was to characterize estrogen-induced circRNAs with potential functions in modulating muscle development in sheep. Using high-throughput RNA sequencing, we first systematically investigated the expression profiles and functions of circRNAs in the *longissimus dorsi* muscle of 8-month-old small-tailed Han sheep with and without ovaries. One significantly upregulated circRNA (novel_circ_0011822) in intact ewes, which was named circFAM171A1 on the basis of its source gene, was highlighted. Bioinformatics analysis revealed that circFAM171A1-oar-miR-485-5p-MAPK15 could form a ceRNA, in which MAPK15 is an important gene in the MAPK signaling pathway. In addition, we verified the influence of estrogen-induced ceRNAs on the growth and progression of sheep myoblasts in vitro. These findings may help to elucidate the molecular mechanisms by which estrogen regulates muscle progression in sheep.

Materials and methods

Ethics statement

The study was approved by the IAS-CAAS Animal Ethics Committee under approval number IAS2019-63. In strict compliance with relevant regulations, we are committed

to promoting animal science research to contribute to the development of agriculture in China.

Sample collection and preparation

In this study, we selected 10 small-tailed Han sheep ewes aged 2 months from Wulat Zhongqi Farm, Bayannur City, Inner Mongolia Autonomous Region, China. For comparative observations, the sheep were randomized into two groups: the ovariectomized group (n = 5, OR-STH) and the sham surgery group (n = 5, STH). There were no significant differences between the two groups in terms of height, weight, or age. After surgery, both groups of sheep were kept in the same feeding environment. Over a 6-month period, sheep weights were measured, and tissue samples were collected from the *longissimus dorsi* muscle. The mean body weights were 72.4 ± 1.86 kg and 88.4 ± 3.97 kg in the OR-STH and STH groups, respectively ($P < 0.05$). The estrogen levels in the serum of the sheep were 28.71 ± 2.73 pg/mL and 12.23 ± 0.82 pg/mL in the STH group and OR-STH group, respectively ($P < 0.05$). All the tissue samples were immediately frozen in liquid nitrogen to ensure their stability. The samples were subsequently stored in a cryogenic environment at −80 °C until further analysis.

Library preparation and Illumina sequencing

In this study, we first extracted total RNA from 10 muscle tissue samples using TRIzol reagent (Invitrogen, Carlsbad, CA, USA) according to the manufacturer's instructions. The total amount of RNA extracted was 2 μg (concentration ≥ 300 ng/μL, OD260/280 between 1.8 and 2.2), which was used as the raw material for constructing the miRNA and cDNA libraries. To remove ribosomal RNA (rRNA), we used the Epicenter Ribo-Zero™ rRNA Removal Kit (Epicenter, Madison, WI, USA). After rRNA removal, we constructed sequencing libraries using the NEBNext® Ultra™ Directional RNA Library Prep Kit for Illumina® (NEB, Ipswich, MA, USA) following the manufacturer's instructions. Throughout the process, we also purified the products using the AMPure XP system and assessed the quality of the library via gel electrophoresis and the NanoDrop 2000, Qubit 2.0, and Agilent Bioanalyzer 2100 systems. Finally, the libraries were sequenced on an Illumina HiSeq 2500 platform, yielding 150 bp paired-end reads.

Identification of differentially expressed circRNAs and mRNAs

First, we approximated the levels of expression of circRNAs in the constructed muscle tissue libraries via Illumina sequencing data and the FPKM/readcount values. To ensure the accuracy of the results, two software programs, find_circ and CIRI2, were used for circRNA identification, and the intersection was taken for the final results. To identify mRNA, we used the DE-Seq R software package (version 4.2.1). For the DE-Seq analysis, we used a threshold of a q value less than 0.05 and a |log2FoldChange| greater than 1 to adjust for mRNA. Next, we used the DEG-seq R package to analyze differentially expressed circRNAs (DECs) on the basis of normalized reads per thousand bases per million (TPM) values. During the analysis, we modified the q value and set the thresholds for significant DECs as a q value less than 0.05 and a |log2FoldChange| greater than 1. This series of analyses provided us with information about the differential expression of circRNAs in muscle tissues as well as the related genes, which provided an important basis for further studies. For a complete list of circRNAs see Supplementary Table S1.

Comprehensive functional enrichment analysis

In the present study, we used functional annotation to analyze DE circRNA host genes on the basis of GO and KEGG annotations. First, for the source genes, we performed GO annotation on the basis of the corresponding genes and their GO annotations in NCBI. This information was stored in the following database: https://ftp.ncbi.nlm.nih.gov/gene/DATA/gene2go.gz. Next, we used KOBAS software to test the statistical enrichment of host genes associated with DE circRNAs in the KEGG pathway [37]. To determine the significance of the enrichment analysis, we set a threshold of $P < 0.05$. This series of functional annotation analyses helped us to gain a deeper understanding of the functions of DE circRNAs in organisms and the roles of their related genes in specific pathways.

ceRNA and PPI networks

We first constructed a ceRNA network based on predicted circRNA, miRNA and mRNA binding sites from whole-transcriptome sequencing data and then constructed a circRNA−miRNA−mRNA interaction network via Cytoscape software. This step helped us understand the functions of circRNAs in organisms and their interactions with other genes. Next, we constructed protein−protein interaction (PPI) networks of the differentially expressed genes (DEGs) using STRING (version 11.5, https://string-db.org/). For PPI analysis, we used the STRING database v11.5 (species: *Ovis aries*). To construct the PPI network, we collected target genes from the database and selected protein pairs with scores greater than 700 from the STRING database. Finally, we used Cytoscape software to visualize the protein pairs. This series of analyses helped us gain insight into the interactions between DEGs, providing strong support for

studying the physiological functions of organisms and the mechanisms of disease occurrence.

Immunofluorescence (IF)

We first inoculated sheep primary myoblasts in 6-well plates maintained at a population density of 1×10^6 cells per well, with each group containing three replicates. Next, the polylysine-treated glass coverslips were placed in 6-well plates and removed after 16 h. To fix the cells, we treated them with 4% formaldehyde for 15 min and then washed them with PBS 3 times for 3 min each. Next, the samples were incubated with 10% goat serum (China) for 30 min. For immunofluorescence staining, the samples were incubated with Desmin (1:500) and MYOD1 (1:500) antibodies (Proteintech, USA) overnight at 4 °C. After the incubation was complete, the membrane was washed with PBS five times for 5 min each. Next, of the samples were incubated with fluorescent IgG (1:2000) (Saixin, China) for 1 h at 37 °C. Finally, DAPI (Beyotime, China) was added to stain the nuclei for 5 min, after which the cells were washed 5 times for 5 min each. Through this series of experiments, we successfully examined sheep primary myoblasts, which provided the basis for subsequent studies.

Ribonuclease R (RNase R)

One microgram of sheep muscle tissue RNA was added to RNase R reagent (1 U/μg) and incubated at 37 °C for 10 min. The cDNA was reverse transcribed from RNase R processed RNA and control pretreated RNA, and RT−qPCR was utilized to measure the expression of circRNAs and the corresponding linear transcripts.

Fluorescence in situ hybridization (FISH)

A FISH kit SA-Biotin System (JiMa, Shanghai, China) and a circFAM171A1 probe mixture (Cy3 labeled) were used (Table 1). FISH was conducted according to the manufacturer's instructions to assess the localization of circFAM171A1 in sheep myoblasts. The procedure was as follows: the cells

Table 2 Primer information for RT−qPCR

Gene name	Primer SEQUENCE (5′−3′)	Tm (°C)
MAPK15	F: GGAGGAGGCAGGCGTGTAAG R: TCTCTGGCAGGGCTCAAACC	60
PCNA	F: TTGAAGAAAGTGCTGGAGGC R: TTGGACATGCTGGTGAGGTT	60
Pax7	F: CGTGCCCTCAGTGAGTTCGA R: CCAGACGGTTCCCTTTGTCG	60
CDK2	F: AAGTGGCTGCATCACAAGGA R: CAAGCTCCGTCCATCTTCAT	60
circFAM171A1	F: CGAGGATTAGATGGAAACGG R: AGAAAGGCGGTCAGGTCACT	60
oar-miR-485-5p	F: AGAGGCTGGCCGTGATGA ATT R: CAGTTTTTTTTTTTTTTGGG CAG	60
β-actin	F: AGCCTTCCTTCCTGGGCA TGGA R: GGACAGCACCGTGTTGGC GTAGA	60
U6	F: AACGCTTCACGAATTTGCGT R: CTCGCTTCGGCAGCACA	60
GAPDH	F: CACGGCACAGTCAAGGCAG R: AGATGATGACCCTCTTGGCG	60
novel_circ_0004268	F: ATGTTATACCCCAGCCCAAA R: GAATCCAAAGTCCCAGCCAC	60
novel_circ_0009805	F: AACATGAAGCGTATGTCA CAG R: TTCTTCTTCCCGTTCTACTGA	60
novel_circ_0015927	F: AACAACAGCATCTTCTGG GTA R: GGACTCTAAGAATCCAAA ACC	60
novel_circ_0006391	F: AGTTCATCCAGATGGGCAGC R: GACCAGTTTAACCAGCGTCC	60
novel_circ_0002443	F: GCTGACCTCCTGAAAGACCC R: GAGTGTTGTTCTTCACGGGG	60
novel_circ_0006225	F: GGTGGGAAGAAGGCGAAA TAC R: TTCATTATGGCTCCACTTTGC	60
novel_circ_0005017	F: TTGCCAAACTAACATGGA ATC R: CCGATGTTCTGAAAATGA TGA	60

Table 1 The probe sequences used for multicolor fluorescence in situ hybridization

Name	Marker	Sequence
circFAM171A1	Cy3	5′ GTGCCCGGCCACAGCCTCGAGTACATTTCC AGAGAAGAGCC CTGCGGCTGCCAGAGAACACCAGCTACAGT GACCTGACCGCCT TTCTCACGGCCGCCAGCTCTCCCTCCGAGG TGGACGGCTTTCCT TATTTGCGAGGATTAGATGGAAACGGAACA G 3′
18S		5′ CTGCCTTCCTTGGATGTGGTAGCCGTTTC 3′
NC		5′ TGCTTTGCACGGTAACGCCTGTTTT 3′

Table 3 Statistics on the yield and quality of raw sequencing data from 10 sheep

Sample	Raw reads number	Clean reads number	GC_content	Q30	Uniquely mapped	Aligned rate
OR_STH_1	104,585,290	95,544,247	49.18%	92.55%	88,502,315	84.62%
OR_STH_2	101,968,696	93,513,704	50.12%	93.03%	85,876,093	84.22%
OR_STH_3	100,490,536	90,061,492	50.55%	92.42%	83,926,739	83.52%
OR_STH_4	113,484,726	102,438,833	51.03%	91.78%	94,625,925	83.38%
OR_STH_5	96,930,428	84,250,266	57.00%	91.14%	76,198,353	78.61%
STH_1	105,677,792	96,351,036	49.63%	92.89%	89,110,737	84.32%
STH_2	99,401,202	92,321,713	49.57%	93.12%	85,175,337	85.69%
STH_3	105,305,476	95,083,678	48.00%	93.21%	89,194,000	84.70%
STH_4	101,215,956	92,765,887	49.70%	92.88%	85,287,779	84.26%
STH_5	97,234,736	90,305,800	49.72%	92.93%	82,470,400	84.82%

were cultured in 6-well plates overnight, stabilized with 4% paraformaldehyde for 15 min at room temperature, incubated with probe solution (1 µL of 1 µM biotin probe + 1 µL of 1 µM SA-Cy3 + 8 µL of PBS) added to the medium for 30 min at 37 °C, and placed in an incubator at 37 °C overnight (12–16 h) in the dark to allow hybridization. The cells were stained with DAPI solution (2 µg/mL) for 15 min at room temperature in the dark. An anti-fluorescence quenching blocker was then added. Images were obtained via a computerized laser scanning confocal microscope.

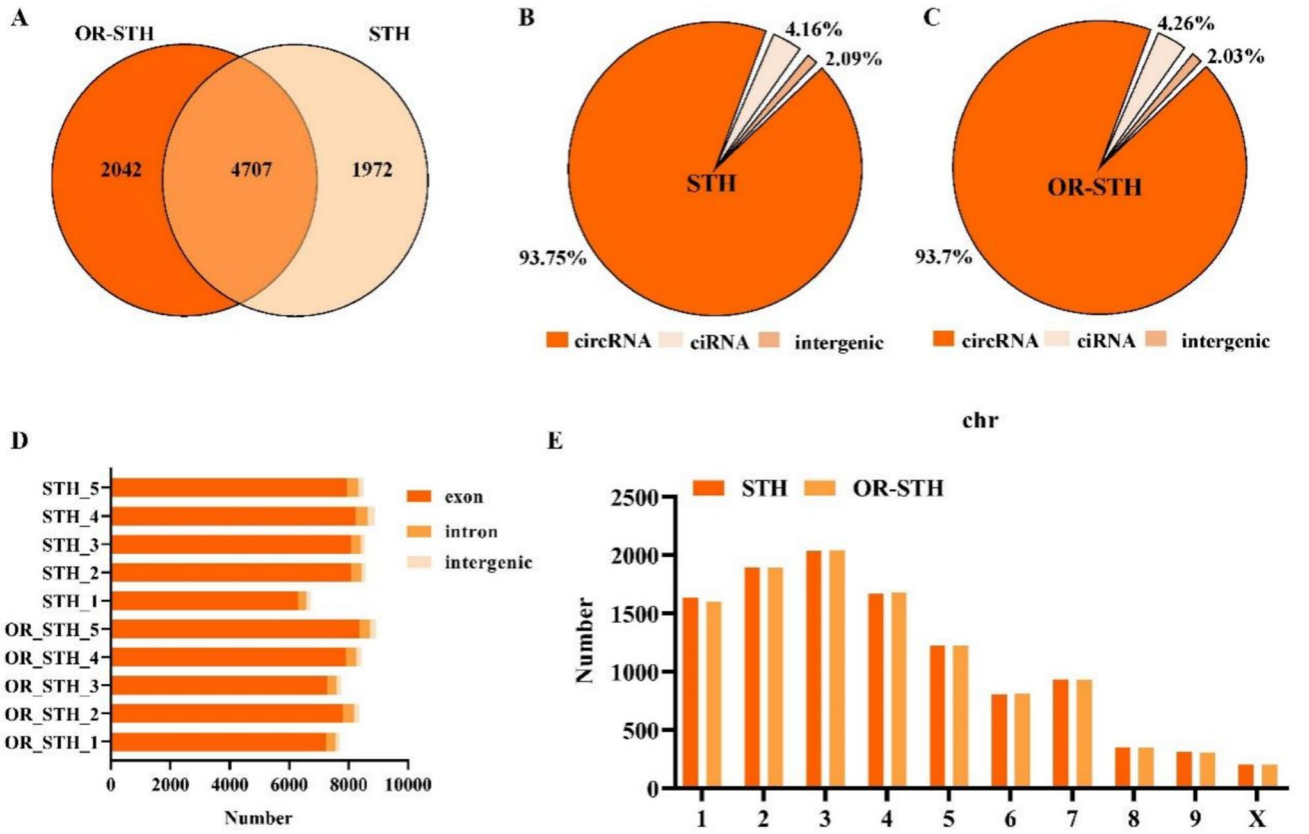

Fig. 1 Basic characteristics of circRNAs in the muscle tissue of small-tailed Han sheep. **A** Venn diagram of different circRNAs found in OR-STH and STH; the OR-STH group library contained 2042 circRNAs, and the STH group library contained 1972 circRNAs. **B** Types of circRNAs associated with STH. **C** Types of circRNAs associated with OR-STH. **D** CircRNA functional region statistics, with exons predominating. (E) Density statistics of the circRNAs on the OR-STH and STH chromosomes revealed that most of the genes were enriched on chromosomes 1, 2, 3 and 4. N = 5

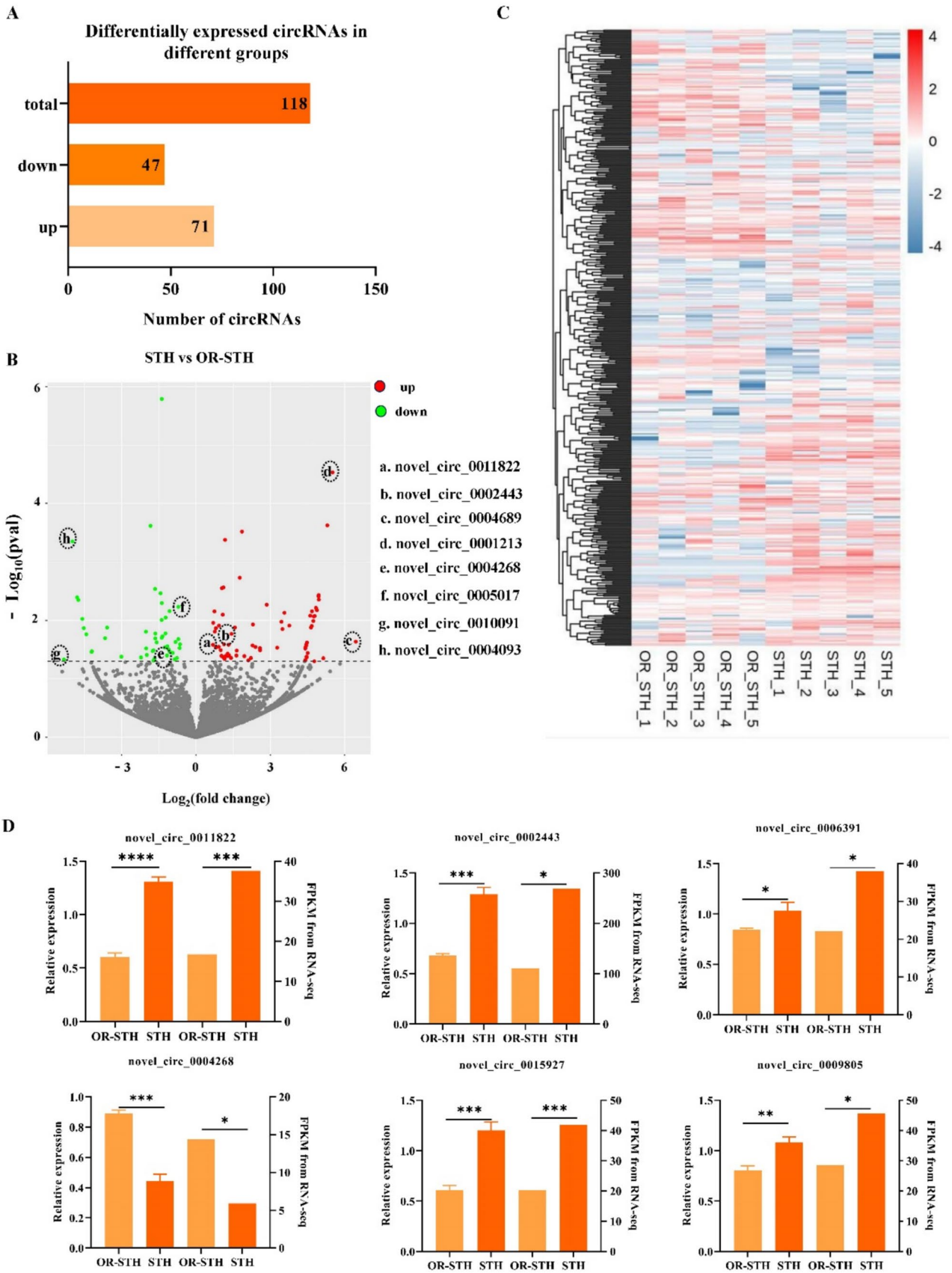
A
Differentially expressed circRNAs in different groups
total
down
up
118
47
71
0
50
100
150
Number of circRNAs
B
STH vs OR-STH
up
down
a. novel_circ_0011822
b. novel_circ_0002443
c. novel_circ_0004689
d. novel_circ_0001213
e. novel_circ_0004268
f. novel_circ_0005017
g. novel_circ_0010091
h. novel_circ_0004093
- Log10(pval)
Log2(fold change)
C
OR_STH_1
OR_STH_2
OR_STH_3
OR_STH_4
OR_STH_5
STH_1
STH_2
STH_3
STH_4
STH_5
D
novel_circ_0011822
novel_circ_0002443
novel_circ_0006391
novel_circ_0004268
novel_circ_0015927
novel_circ_0009805
Relative expression
FPKM from RNA-seq
OR-STH
STH

◂**Fig. 2** Differentially expressed circRNAs. **A** The bar graph showed that a total of 118 DE circRNAs were identified between OR-STH and STH groups. **B** Scatter plot of differentially expressed circRNAs. **C** Cluster heatmap of differentially expressed circRNAs. The horizontal coordinates are the samples, and the vertical coordinates are the genes screened out by differential expression. Different colors indicate different gene expression levels. The color changes from blue to white to red; red indicates highly expressed genes, and blue indicates genes with low expression. (D) RT−qPCR results of different circRNAs in the OR-STH and STH groups. N = 3; * $P < 0.05$; ** $P < 0.01$; *** $P < 0.001$; ns, not significant

Nucleoplasmic separation

Sheep myoblasts were inoculated at a density of $\leq 3 \times 10^6$ in 6-cm culture dishes, and after 24 h of cell culture, the cells were washed with PBS twice, and the PBS was discarded. Two hundred microlitres of prechilled buffer J was added to the culture dish to cover the cell surface, the mixture was allowed to cool for 5 min, the lysis products were collected, the mixture was moved to an RNase-free sponge tube, and the mixture was centrifuged at 14,000 × g for 10 min at 4 °C. The liquid supernatant (cytoplasmic RNA) was pipetted into another centrifuge tube, 200 μL of buffer SK was added to the precipitate (cytosolic RNA), another 400 μL of buffer SK was added, the mixture was vortexed for 10 s, 200 μL of anhydrous ethanol was added, and the mixture was vortexed for 10 s. The mixture was transferred to a centrifuge column and centrifuged at 6000 rpm for 1 min at 4 °C; the supernatant was discarded, and the column was returned to the centrifuge tube. A total of 400 μL of wash solution A was added, and the mixture was centrifuged at 14,000 × g and 4 °C for 1 min. The supernatant was discarded, the column was washed once, the mixture was placed back into the collection tube, and the mixture was centrifuged at 14,000 × g and 4 °C for 2 min. Then, 50 μL of elution buffer E was added, the mixture was centrifuged at 6000 rpm and 4 °C for 2 min, followed by centrifugation at 14,000 × g and 4 °C for 1 min. The RNA concentration was then detected, and the samples were stored at −80 °C.

Expression validation by RT−qPCR

mRNA and miRNA back-transcription were performed using the HiScript® IiI All-in-one RT SuperMix kit (Vazyme, Nanjing, China) and the miRNA first-strand cDNA synthetic kit (Vazyme, Nanjing, China). RT-qPCR was performed on a RocheLight Cycler® 480 II system (Roche Applied Science, Mannheim, Germany), and the mRNA and miRNA were extracted using the Taq Pro Universal SYBR qPCR Master Mix (Vazyme). RT-qPCR was performed on a RocheLight Cycler® 480 II system (Roche Applied Science, Mannheim, Germany), and mRNAs and miRNAs were extracted using Taq Pro Universal SYBR qPCR Master Mix (Vazyme). The RT-qPCR procedure was as follows: preliminary denaturation at 95 °C for 5 min, denaturation at 95 °C for 5 s, and degradation at 60 °C for 30 s for 35 cycles. The data were analyzed via the $2^{-\Delta\Delta Ct}$ method, with the sheep β-actin and U6 genes used as internal control genes. The relative expression was analyzed by a *t* test of dependent samples, and the significance of differences was analyzed by SPSS 20.0. The primers for RT−qPCR were designed by Primer 5 software and constructed by Sangon Biotech Co. (Shanghai). The primer sequences are listed in Table 2.

Cell culture

The *longissimus dorsi* muscle tissues from both surfaces of the fetal spine of 90-day-old small-tailed Han sheep were isolated under aseptic conditions, and combinations of connective tissues and blood tubes were removed and then washed with PBS (2% penicillin/streptomycin). The muscle samples were pelleted and digested with 0.25% trypsin (Solarbio, Beijing, China) for 18 h at 4 °C and then cultured in an incubator (37 °C, 5% CO_2) for approximately 2 h. The cells were then cultured in the incubator for approximately 2 h. The cells were then incubated for approximately 1 h at 4 °C. The isolated cells were inoculated into 100 mm culture dishes and cultured with complete media (DMEM-F12, 10% FBS and 1% penicillin/streptomycin). After the cells reached more than 90% confluence, they were transferred to 6-well plates for subsequent experiments. The HEK293T cell line was cultivated under the same cultivation requirements.

Plasmid construction and transfection

Overexpression of pcDNA3.1-circFAM171A1 and interference siRNA vectors were designed and synthesized on the basis of the sequence of circFAM171A1. The mimics and inhibitors of oar-miR-485-5p were designed and synthesized on the basis of the sequence of oar-miR-485-5p. MAPK15 overexpressing pIRES2-EGFP-MAPK15 and interfering with si-MAPK15 were designed and synthesized on the basis of the sequence of MAPK15 provided by NCBI. The overexpression and interference vectors, mimics and inhibitors were synthesized by Shanghai Gemma Pharmaceuticals Technology Co. All the vectors were sequenced, and the sheep myoblasts and HEK293T cells were transfected with Lipofectamine 2000 (Invitrogen, Carlsbad, CA, USA) according to the manufacturer's instructions. Cell growth and gene expression were assessed 48 h posttransfection.

Western blot

Proteins in the cell samples were extracted with radioimmunoprecipitation assay (RIPA) buffer (Solebro, Beijing,

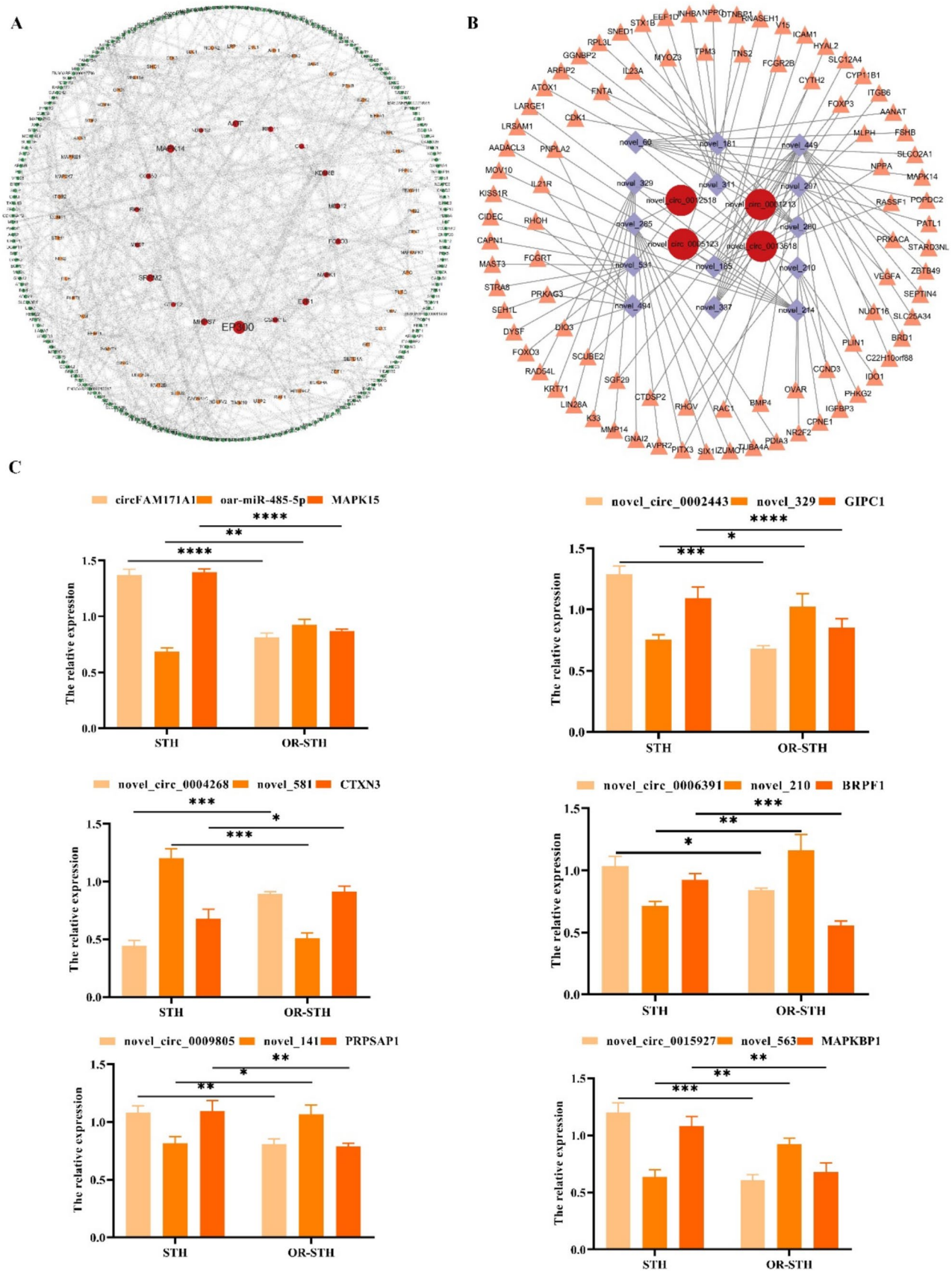
A
B
C
circFAM171A1 oar-miR-485-5p MAPK15
The relative expression
STH
OR-STH
novel_circ_0002443 novel_329 GIPC1
novel_circ_0004268 novel_581 CTXN3
novel_circ_0006391 novel_210 BRPF1
novel_circ_0009805 novel_141 PRPSAP1
novel_circ_0015927 novel_563 MAPKBP1

◂**Fig. 3** Analysis of differentially expressed circRNAs, miRNAs and mRNAs. **A** PPI network of differential mRNAs. **B** CircRNA−miRNA−mRNA interaction network. **C** RT−qPCR validation of differentially expressed circRNA-miRNA−mRNA. U6 and β-actin were used as internal controls. N = 3; the data are expressed as the mean ± SD. * $P < 0.05$; ** $P < 0.01$; *** $P < 0.001$; ns, not significant

China) containing 1% PMSF. The protein concentration was measured with a BCA test kit (Solebro, Beijing, China). Proteins were separated on a 10% SDS-polyacrylamide gel (Bio-Rad, Hercules, CA, USA) and then transferred to a polyfluoroethylene membrane. The films were then incubated with specific primary antibodies against PCNA, CDK2 and Pax7 and the corresponding secondary antibodies, and the membranes were color developed with an ultrasensitive ECL chemiluminescent reagent (Biyuntian, Beijing, China), exposed with an Odyssey CLX imaging screen system (Li-COR), photographed and archived. The relative expression level of the target protein was determined by the ratio of the gray value of the target protein to that of GAPDH/β-tubulin.

Cell proliferation assay

The proliferation of sheep myoblasts was detected with a Cell Counting Kit-8 (CCK-8) (Biyun Tian, Beijing, China) according to the manufacturer's instructions. After the transfection of related plasmids, 10 μL of CCK-8 was added to each well at 0, 6, 12, 24, and 48 h. After 2 h of incubation in an incubator, the proliferation rate of the myoblasts was calculated by measuring the absorbance at 450 nm with an enzyme marker. The proliferation of sheep myoblasts was detected with an EdU Cell Proliferation Detection Kit (Biyuntian, Beijing, China). After plasmid transfection, the cells were cultured for 48 h. EdU working solution preheated at 37 °C was added, and the cells were transfected for 2 h. The findings were visualized and photographed under a fluorescence microscope (Leica, Germany).

Dual-luciferase reporter assay

Sheep myoblasts were inoculated evenly into 24-well cell culture plates. When the desired cell density was reached, psiCHECK2-circFAM171A1-WT- and psiCHECK2-circFAM171A1-MUT-cotransfected cells were cotransfected with psiCHECK2- MAPK15-WT or psiCHECK2-MAPK15-MUT and oar-miR-485-5p mimics or NC mimics. CircFAM171A1-MUT-oar-miR-485-5p-transfected cells. Serum luciferase detection was performed according to the manufacturer's directions using a Dual-Luciferase Detection Kit (Vazyme, Nanjing, China). Luciferase activity was recorded 48 h after transfection and measured with a multimode microtitration system (EnS pire, Perkin Elmer, USA).

RNA pull-down assay

A pull-down assay with biotinylated miRNA was performed. Briefly, 3′-end biotinylated oar-miR-485-5p mimic or control RNA (50 nM, GenePharma, Shanghai, China) was transfected into SMs. After 24 h, the cells were washed with phosphate-buffered saline (PBS) and harvested using lysis buffer supplemented with 50 U of RNase OUT. The biotin-coupled RNA complex was collected with a Dynabeads MyOne Streptavidin C1 kit (Invitrogen, Carlsbad, CA, USA) according to the manufacturer's protocol. The bead-bound RNA (pull-down RNA) was isolated using TRIzol reagent. The abundance of circFAM171A1 in the isolated fractions was evaluated by RT-qPCR analysis. Each experiment was performed three times.

Estradiol assay

The 17β-estradiol (10 mM/mL, DMSO) was purchased from MedChe Express (New Jersey, USA). To establish the best concentration for the experiment, estradiol was diluted in a gradient (0 nM, 1 nM, 10 nM, and 100 nM) and then added to the myoblast culture medium along with the suspended cells. The cells were cultured in gradient-diluted estradiol medium for 48 h, after which RNA and proteins were extracted.

Statistical analysis

All analyses were performed with at least three technical replications. The data are expressed as the average ± standard error of measurement (SEM) and were plotted with GraphPad Prism software. Statistical data were analyzed using SPSS 20 (SPSS INC. Chicago, IL, USA) software, with separate samples t tests for making comparisons between two datasets and one-way ANOVA for making comparisons between more than two datasets. Statistical significance is expressed as ** $P < 0.01$, * $P < 0.05$.

Results

CircRNA expression profile in the *longissimus dorsi* of ovariectomized and sham-operated small-tailed Han sheep

A total of 1,026,294,838 raw reads were derived from 10 muscle sequencing libraries from the OR-STH and STH groups, and 932,636,656 clean reads, accounting for 90.87%

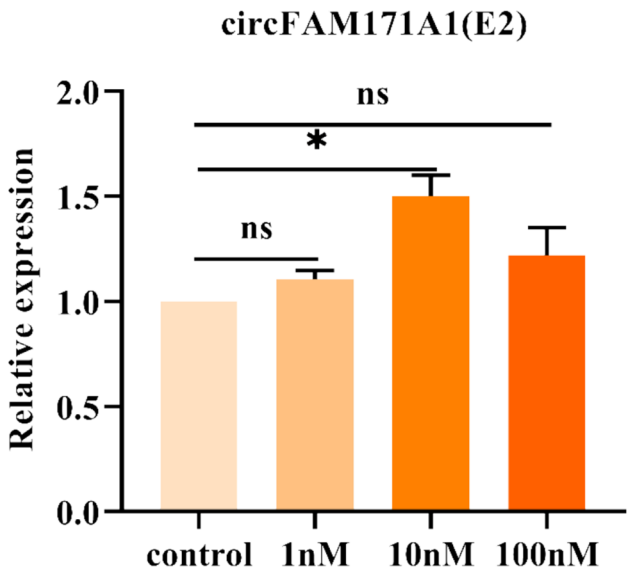

Fig. 4 The expression of circFAM171A1 in sheep myoblasts was highest at 10 nM after the addition of 0 nM, 1 nM, 10 nM and 100 nM estradiol. β-actin was used as an internal control. N = 3; the data are expressed as the mean ± SD. ns, not significant, * $P < 0.05$

of the raw data, were obtained after quality control (Table 3). In addition, the Q30 values were greater than 91.14%, indicating good sequencing quality, and the average net read rate was 83.81% (from 78.61 to 85.69%) for only mapping to the sheep genome. Following the removal of ribosomal RNA (rRNA), 8,721 potential candidate circRNAs were identified (Supplementary Table S2). To identify circRNAs with potential functions in sheep muscle development, we counted the identified circRNAs. The findings revealed that the OR-STH group library contained 2,042 circRNAs and that the STH group library contained 1,972 circRNAs (Fig. 1A). The major circRNA types identified in the study were all exonic (OR_STH: 93.70%; STH: 93.75%), lasso-type (OR_STH:4.26%; STH:4.16%) and intergenic (OR_STH: 2.03%; STH:2.09%; Fig. 1B, C). The circRNAs were generated primarily from exon splicing, with a smaller share of intronic and regenerative splicing (Fig. 1D). The statistics of circRNA density per chromosome indicated that circRNAs were located on chromosomes 1 to 9, with the proportion of circRNAs on chromosomes 1, 2, 3, and 4 being the highest (approximately 42%) (Fig. 1E). The distribution of genes on chromosomes is shown in supplementary materials Figure S1A and S1B.

Differential expression analysis of circRNAs

The number of circRNAs expressed by each individual was calculated and standardized to SRPBM. The expression of circRNAs was normalized to SRPBM expression on the basis of the normalized expression, |log2 (foldchange)|> 1, P value < 0.05. A total of 118 DE circRNAs (71 upregulated and 47 downregulated) were identified when OR-STH was compared with STH (Fig. 2A). The overall distribution of the differentially expressed circRNAs is shown in the scatter plot in Fig. 2B, the cluster heatmap in Fig. 2C and the box plot and violin plot in supplementary materials Figure S1C and S1D. To ensure the precision of the RNA-seq protocol, we randomly selected eight circRNAs that were differentially expressed and designed specific RT−qPCR primers in the circRNA boundary region. The levels of DE circRNA expression measured by RT−qPCR and RNA−seq showed the same trend (Fig. 2D). This result indicates that the RNA-seq acquisition and subsequent organization of the data in this study are reliable. In addition, to provide more information about the functions of circRNAs in muscle growth and development in sheep, we performed GO and KEGG analyses of the host genes (supplementary materials Figure S1E and S1F).

Analysis of ceRNA regulatory networks (circRNA-miRNA−mRNA networks)

A combination of differentially expressed circRNAs (DECs), differentially expressed miRNAs (DEMs), and differentially expressed mRNAs (DEGs) were identified from sheep *longissimus dorsi* muscle by analyzing whole-transcriptome data to generate a ceRNA regulatory network. A total of 41 circRNA−miRNA pairs and 3,499 miRNA−mRNA pairs were filtered by comparing negatively correlated circRNA−miRNA pairs and miRNA−mRNA pairs in the OR-STH and STH data ($P < 0.05$). Four randomly selected differentially expressed circRNAs with more or less than three binding sites and 14 miRNAs and 90 mRNAs, all of which were differentially expressed, were selected, resulting in the construction of an interaction network: the circRNA−miRNA−mRNA interface network (Fig. 3A). The screened differential genes were analyzed against the host genes using the STRING database. We selected > 700-point protein pairs and constructed protein–protein interaction (PPI) networks of host genes using Cytoscape (Fig. 3B). Six sets of differential circRNA-miRNA−mRNA pairs were subsequently chosen for RT−qPCR: circFAM171A1-oar-miR-485-5p-MAPK15, novel_circ_0002443-novel_329-GIPC1, novel_circ_0009805-novel_141-PRPSAP1, novel_circ_0006391-novel_210-BRPF1, novel_circ_0015927-novel_563-MAPKBP1. RT−qPCR confirmed that the changes of circRNA, miRNA and mRNA expression levels in sheep muscle tissues were consistent with the RNA-seq data and was negatively correlated ($P < 0.05$) (Fig. 3C).

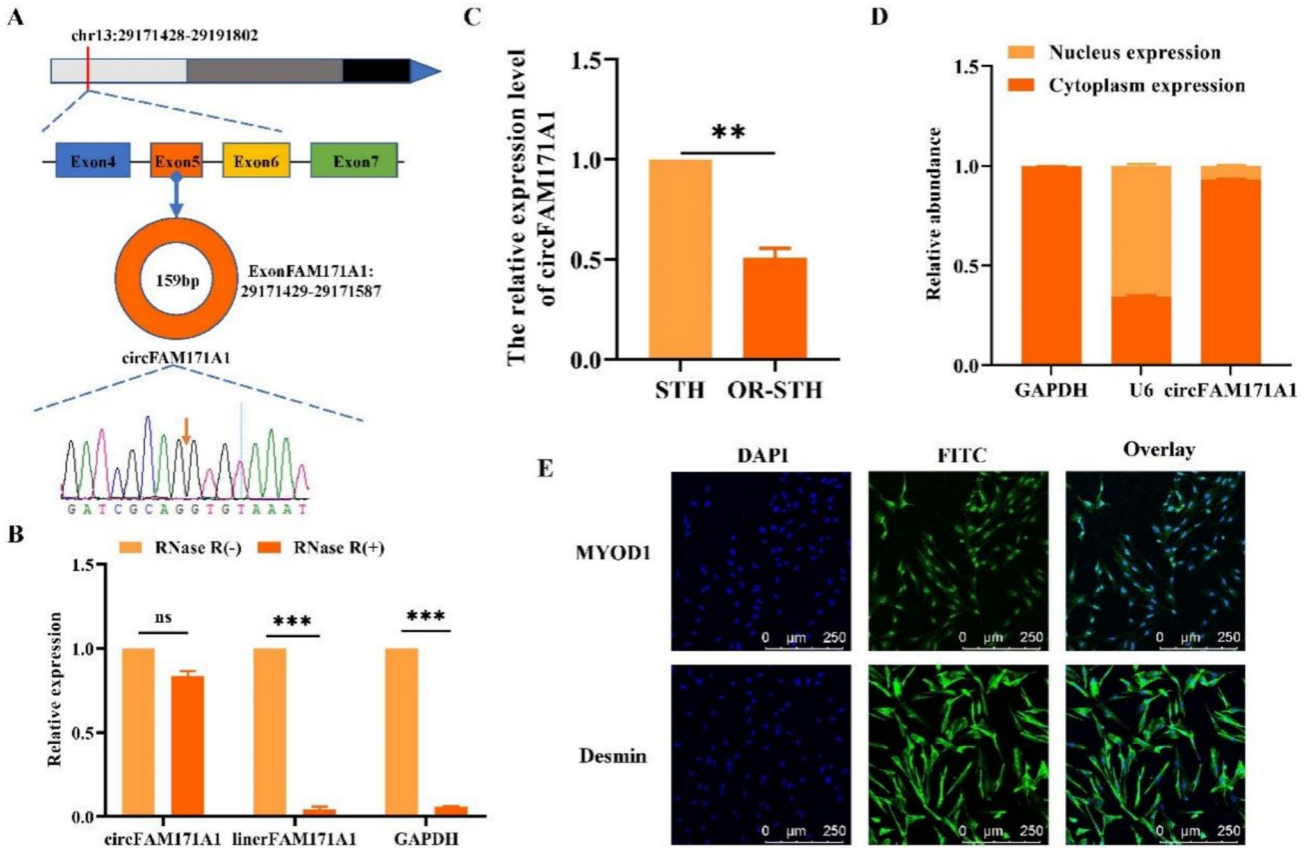

Fig. 5 Identification and expression level analysis of circFAM171A1. **A** Schematic showing the circularization of FAM171A1 to form circFAM171A1. The head-to-tail splicing of circFAM171A1 was identified via Sanger sequencing. **B** Resistance to RNase R was tested by RT−qPCR, which revealed that circFAM171A1 was more stable than linear FAM171A1. **C** The expression levels of circFAM171A1 in the STH and OR-STH groups. (D and Figure S2) Nucleoplasmic separation (**D**) and FISH (Figure S2) analysis revealed that circFAM171A1 was localized mainly in the cytoplasm. **E** Immunofluorescence confirmed that the cells were sheep myoblasts. N = 3; * $P < 0.05$, ** $P < 0.01$, *** $P < 0.001$; *ns* not significant

Estrogen induced circFAM171A1 production in sheep myoblasts

RNA-seq and RT−qPCR revealed that the abundance of circFAM171A1 in the STH group was clearly greater than that in the OR-STH group, suggesting that the difference in the expression level of circFAM171A1 may be a result of estrogen induction. To clarify the above results, we added different concentrations of estrogen to isolated myoblasts in vitro to detect the circulation of circFAM171A1 in myoblasts. The findings indicated that the level of circFAM171A1 increased significantly in all groups after the addition of estrogen, and when the concentration reached 10 nM, the expression level of circFAM171A1 was significantly greater than that in the other groups (Fig. 4). This result suggests that the level of circFAM171A1 expression in sheep myoblasts was indeed affected by estrogen.

Identification of circFAM171A1 as a candidate circRNA

Previous research has demonstrated that circRNAs can eliminate the potential for miRNAs to negatively affect the expression of target genes [38, 39]. CircFAM171A1 is 159 bp long and originates from exon 5 of the gene encoding the protein FAM171A1. The reverse splice junction of circFAM171A1 was verified via Sanger sequencing (Fig. 5A). The level of circFAM171A1 expression was not markedly reduced in sheep myoblasts after RNase R treatment, but the levels of linear FAM171A1 and GAPDH mRNA expression were reduced (Fig. 5B). Next, we examined the expression of circFAM171A1 in muscle tissues from both ovariectomized and sham surgery in small-tailed Han sheep via RT−qPCR. The results revealed that circFAM171A1 was expressed in muscle tissues from both the OR-STH and STH groups and that the expression level of circFAM171A1 was significantly greater in the STH group than in the OR-STH group, which is consistent with our

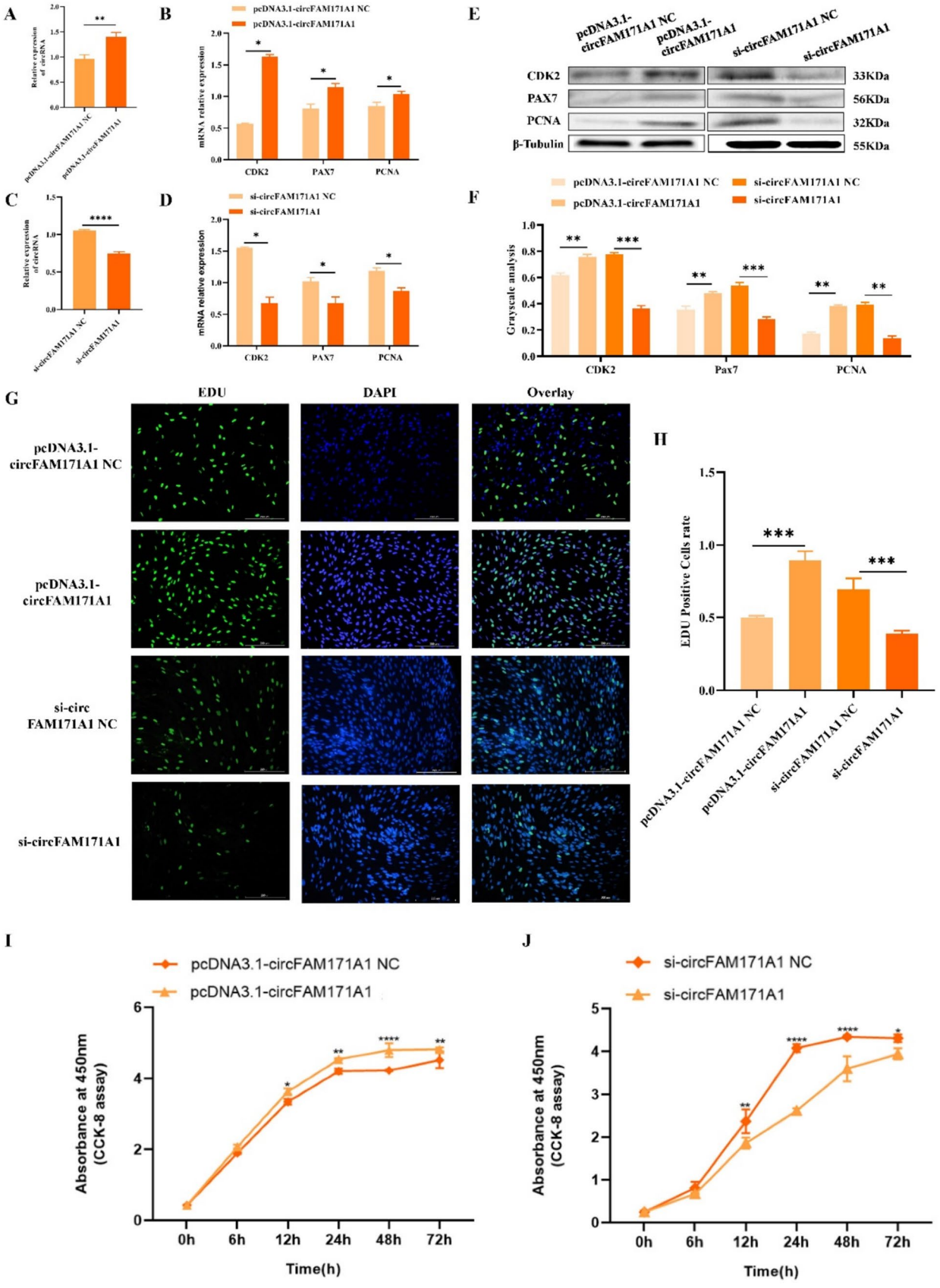
A
Relative expression of circRNA
pcDNA3.1-circFAM171A1 NC
pcDNA3.1-circFAM171A1
B
pcDNA3.1-circFAM171A1 NC
pcDNA3.1-circFAM171A1
mRNA relative expression
CDK2
PAX7
PCNA
C
si-circFAM171A1 NC
si-circFAM171A1
D
si-circFAM171A1 NC
si-circFAM171A1
E
pcDNA3.1-circFAM171A1 NC
pcDNA3.1-circFAM171A1
si-circFAM171A1 NC
si-circFAM171A1
CDK2 33KDa
PAX7 56KDa
PCNA 32KDa
β-Tubulin 55KDa
F
Grayscale analysis
G
EDU
DAPI
Overlay
pcDNA3.1-circFAM171A1 NC
pcDNA3.1-circFAM171A1
si-circ FAM171A1 NC
si-circFAM171A1
H
EDU Positive Cells rate
I
pcDNA3.1-circFAM171A1 NC
pcDNA3.1-circFAM171A1
Absorbance at 450nm (CCK-8 assay)
0h 6h 12h 24h 48h 72h
Time(h)
J
si-circFAM171A1 NC
si-circFAM171A1
Absorbance at 450nm (CCK-8 assay)
Time(h)

◂**Fig. 6** Effect of circFAM171A1 on the proliferation of sheep myoblasts. **A** circFAM171A1 was successfully overexpressed in primary sheep myoblasts. **B** The expression of CDK2, PCNA and Pax7 was detected via RT−qPCR after transfection with the pcDNA3.1-circFAM171A1 vector. **C** circFAM171A1 was successfully inhibited in primary sheep myoblasts. **D** The expression of CDK2, PCNA and Pax7 was detected by RT−qPCR after transfection with the si-circFAM171A1 vector. **E** and **F** Protein expression of CDK2, PCNA and Pax7 was detected by Western blotting after transfection with the pcDNA3.1-circFAM171A1 and si-circFAM171A1 vectors. **G** and **H** EdU (scale bar, 200 μm) was used to measure the proliferative capacity. (I and J) CCK8 assay for proliferation of pcDNA3.1-circFAM171A1- and si-circFAM171A1-transfected sheep muscle cells. N = 3; the data are shown as the means ± SEMs. * $P < 0.05$, ** $P < 0.01$, *** $P < 0.001$, **** $P < 0.0001$. ns, not significant

RNA-seq data (Fig. 5C). Subsequent RNA nucleoplasmic isolation assays revealed that circFAM171A1 was localized predominantly in the cytoplasm (more than 80%) and to a lesser extent in the nucleus (Fig. 5D). RNA fluorescence in situ hybridization experiments further confirmed these findings (Figure S2). Immunofluorescence staining revealed that the myoblast marker MYOD1 was expressed predominantly in the nucleus, whereas Desmin was expressed predominantly in the cytoplasm (Fig. 5E). These results indicate that the circularized form of circFAM171A1 was more stable than the linear transcript RNA, and circFAM171A1 was primarily functional when expressed in the cytoplasm.

Effects of circFAM171A1 on the proliferation of sheep myoblasts

To validate the influence of circFAM171A1 on muscle progression in sheep, we constructed overexpression and interference plasmids for circFAM171A1 and transfected them into sheep primary myoblasts for 48 h. Figure 6A and 6C show that circFAM171A1 overexpression and interference plasmids were effective. The RT−qPCR results revealed that the expression levels of CDK2, Pax7 and PCNA, which are markers of cell proliferation, were significantly increased in sheep myoblasts after overexpression of circFAM171A1, whereas the opposite was observed after inhibition of their expression (Fig. 6B, D). The Western blot results were consistent with the RT−qPCR results (Fig. 6E, F). EdU staining also revealed that circFAM171A1 overexpression significantly increased the number of EdU-positive cells, whereas the opposite effect was observed after circFAM171A1 expression was inhibited (Fig. 6G, H). The CCK-8 results revealed that overexpression of circFAM171A1 significantly increased the viability of sheep myoblasts, whereas inhibition of circFAM171A1 expression had the opposite effect (Fig. 6I, J). These findings indicate that circFAM171A1 promoted the proliferation of sheep myoblasts.

CircFAM171A1 acts as a sponge for oar-miR-485-5p to regulate myoblast proliferation

Cellular localization of circFAM171A1 via nucleoplasmic separation and FISH probes indicated that circFAM171A1 is located mainly in the cytoplasm. When a circRNA is contained in the cytoplasm, it functions mainly by interacting with miRNAs [40]. Therefore, we hypothesized that circFAM171A1 might be a possible sponge for miRNAs. To verify that circFAM171A1 is a ceRNA aimed at miRNAs, we selected miRNAs that participate in the development of sheep myoblasts via transcriptomic data and confirmed the binding relationship between circFAM171A1 and miRNAs via RNA hybridization. We discovered that circFAM171A1 might bind to oar-miR-485-5p, with the binding information shown in Fig. 7A. RT−qPCR revealed that overexpression of circFAM171A1 decreased the expression of oar-miR-485-5p, whereas disruption of circFAM171A1 increased the expression of oar-miR-485-5p (Fig. 7B, C). Next, we constructed plasmids for luciferase reporter assays to validate the binding of circFAM171A1 to oar-miR-485-5p. Dual luciferase reporter assays suggested that oar-miR-485-5p significantly inhibited the Rluc expression of pCK-circFAM171A1-WT in HEK293T cells, yet it had no influence on pCK-circFAM171A1-MUT (Fig. 7D, E). We then performed RNA pull-down experiments, and the results revealed that circFAM171A1 was significantly enriched compared with the negative control (NC) (Fig. 7F). We further confirmed that circFAM171A1 can bind oar-miR-485-5p to regulate myoblast proliferation. RT−qPCR revealed that the mRNA levels of CDK2, Pax7, and PCNA were significantly decreased after transfection of the mimics, whereas the exact opposite was observed after transfection of the inhibitors (Fig. 7G–J). The Western blotting results were consistent with the RT−qPCR results (Fig. 7K, L). In addition, CCK-8 and EdU assays revealed similar changes (Fig. 7M–P). These findings demonstrate that circFAM171A1 can act as a sponge for oar-miR-485-5p and confirmed that oar-miR-485-5p can inhibit the proliferation of sheep myoblasts.

CircFAM171A1 impairs the inhibitory effect of oar-miR-485-5p on MAPK15 expression

To clarify the circRNA-miRNA−mRNA ceRNA mechanism, we investigated the oar-miR-485-5p target gene MAPK15. We examined the expression level of the target gene MAPK15 in sheep muscle. Western blotting revealed that there was a statistically significant difference in MAPK15 protein activity between the OR-STH and STH groups (Fig. 8A). The expression of MAPK15 increased significantly after the overexpression of circFAM171A1 and decreased after circFAM171A1 inhibition, as shown

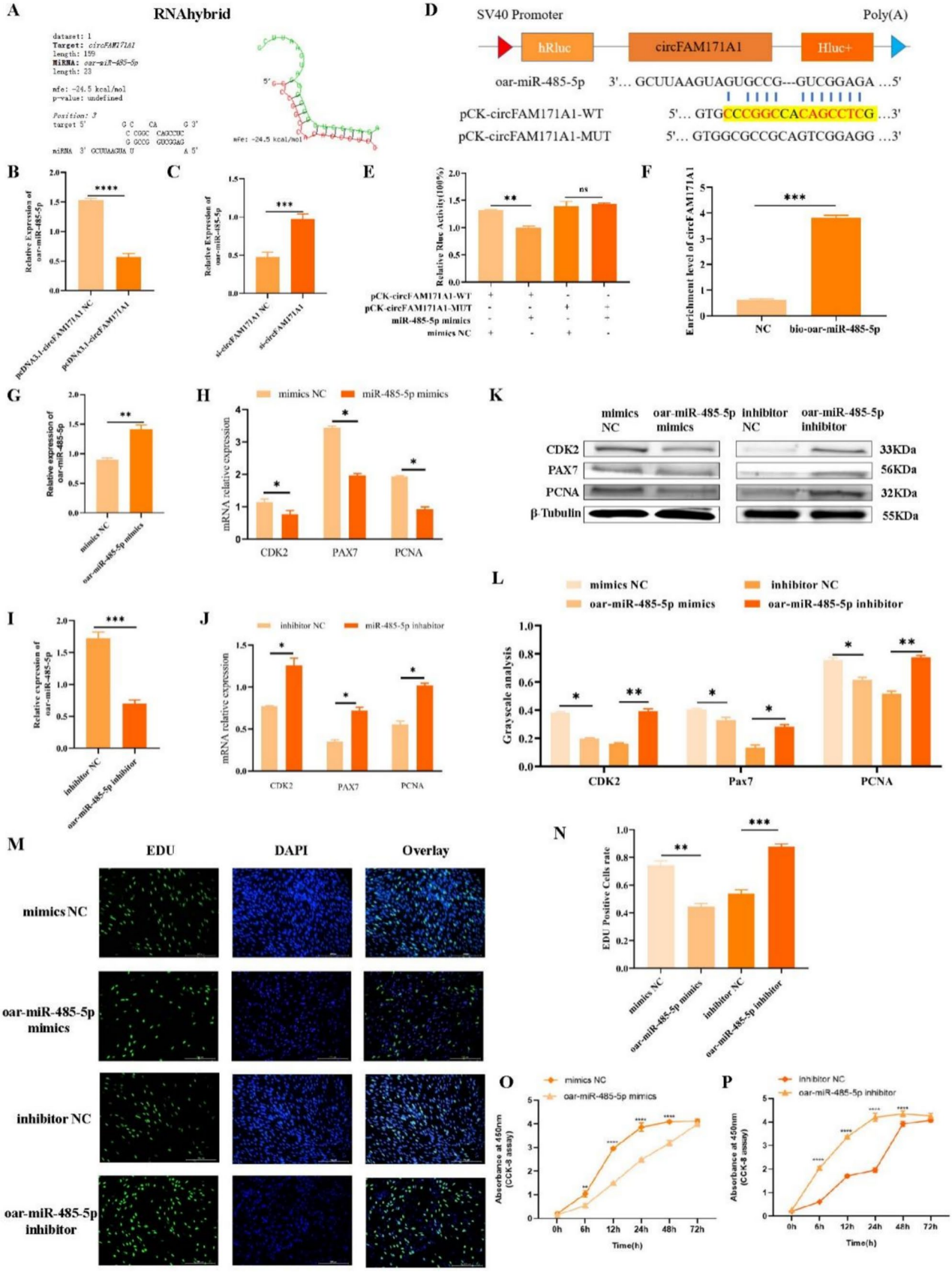
A
RNAhybrid
D
SV40 Promoter
Poly(A)
hRluc
circFAM171A1
Hluc+
oar-miR-485-5p 3'... GCUUAAGUAGUGCCG---GUCGGAGA ...5'
pCK-circFAM171A1-WT 5'... GTGCCCGGCCACAGCCTCG ...3'
pCK-circFAM171A1-MUT 5'... GTGGCGCCGCAGTCGGAGG ...3'
B
C
E
F
G
H
mimics NC
miR-485-5p mimics
K
mimics NC
oar-miR-485-5p mimics
inhibitor NC
oar-miR-485-5p inhibitor
CDK2
PAX7
PCNA
β-Tubulin
33KDa
56KDa
32KDa
55KDa
I
J
inhibitor NC
miR-485-5p inhabitor
L
Grayscale analysis
M
EDU
DAPI
Overlay
N
EDU Positive Cells rate
O
P
Absorbance at 450nm (CCK-8 assay)
Time(h)

◂**Fig. 7** Effect of oar-miR-485-5p on sheep myoblast proliferation. **A** The proposed circFAM171A1 binding site on oar-miR-485-5p was identified using RNAhybrid. **B** Relative expression of oar-miR-485-5p after successful overexpression of circFAM171A1. **C** Relative expression of oar-miR-485-5p after interference with circFAM171A1. **D** Construction of a luciferase expression plasmid with the oar-miR-485-5p binding site in circFAM171A1. **E** Dual luciferase activity assay after co-transfection of oar-miR-485-5p and pCK-circFAM171A1-WT or pCK-circFAM171A1-MUT in HEK293T cell line. **F** RNA pull-down assays were used to detect the relationship between circFAM171A1 and oar-miR-485-5p. **G** and **H** Relative expression of oar-miR-485-5p and the expression of CDK2, PCNA and Pax7 after transfection with oar-miR-485-5p mimics. **I** and **J** Relative expression of oar-miR-485-5p and the expression of CDK2, PCNA and Pax7 after transfection with an inhibitor of oar-miR-485-5p. **K** and **L** Protein expression of CDK2, PCNA and Pax7 after transfection with mimics or inhibitors of oar-miR-485-5p. **M** and **N** After the cells were transfected with mimics or inhibitors of oar-miR-485-5p, EdU (scale bar, 200 μm) was used to measure their proliferative capacity. **O** and **P** Proliferative capacity was measured with a CCK-8 assay after transfection with mimics or inhibitors of oar-miR-485-5p. N = 3; the data are shown as the means ± SEMs. * $P < 0.05$, ** $P < 0.01$, *** $P < 0.001$, **** $P < 0.0001$. ns, not significant

by RT−qPCR (Fig. 8B). The expression of MAPK15 was significantly reduced after oar-miR-485-5p overexpression, whereas the expression of MAPK15 increased after treatment with an inhibitor of oar-miR-485-5p (Fig. 8C). To verify the binding of miRNAs with target genes, we constructed wild-type (WT) and mutant (MUT) psi-CHECK2 plasmids containing the 3′UTR of MAPK15. A dual luciferase activity assay demonstrated that oar-miR-485-5p significantly inhibited the luciferase activity of the wild-type MAPK15′UTR plasmid but not that of the mutant APK15 3′UTR plasmid in HEK293T cells (Fig. 8D). We subsequently synthesized the MAPK15 overexpression plasmid pIRES2-EGFP- MAPK15 and the interference plasmid si-MAPK15, which were subsequently transfected into sheep myoblasts for subsequent validation. We detected a significant increase in MAPK15expression after the transfection of pIRES2-EGFP-MAPK15 (Fig. 8E). Following the transfection of si-MAPK15, we detected a significant decrease in MAPK15 expression. The overexpression or interference of MAPK15 significantly increased or decreased the phosphorylation level of MAPK15, respectively (Fig. 8F). RT−qPCR and Western blot analyses revealed that the overexpression or inhibition of MAPK15 significantly increased or decreased, respectively, the expression of CDK2, Pax7 and PCNA at both the mRNA and protein levels (Fig. 8G, H). EdU and CCK-8 assays revealed that overexpression of MAPK15 increased the proliferation rate of myoblasts, whereas interference with MAPK15 also inhibited the proliferation rate of myoblasts (Fig. 8I, J). These findings indicate that MAPK15 acts in concert with circFAM171A1 in sheep myoblasts and that circFAM171A1 functions as a ceRNA. In summary, circFAM171A1 acts as a sponge of oar-miR-485-5p, weakens its inhibitory effect on MAPK15, and promotes the proliferation of sheep myoblasts.

Estrogen regulates sheep myoblast proliferation through the circFAM171A1/oar-miR-485-5p/MAPK15 pathway

To investigate the influence of estrogen on the proliferation of sheep myoblasts, we examined the proliferation of myoblasts after the addition of 10 nM estradiol. RT−qPCR and Western blotting revealed that the phosphorylation of MAPK15 and the expression of PCNA and CDK2 were significantly increased in the estradiol-treated group (Fig. 9A–D), and the proliferation rate of sheep myoblasts treated with 10 nM estradiol was significantly increased, as indicated by the results of the CCK8 and EdU assays (Fig. 9E–G). To verify the pathway by which estrogen regulates myoblast proliferation, we analyzed the expression levels of oar-miR-485-5p and MAPK15 in sheep myoblasts after the addition of estrogen. The findings indicated that the expression level of oar-miR-485-5p significantly decreased, whereas the protein and mRNA levels of MAPK15 significantly increased ($P < 0.05$) (Fig. 9A–C). These findings indicate that estrogen can facilitate the proliferation of sheep myoblasts through the circFAM171A1/oar-miR-485-5p/MAPK15 pathway (Fig. 10).

Discussion

The important role of estrogen in female mammalian reproduction is well known. However, its functions are not limited to the reproductive system; rather, it also plays important roles in different physiological processes, such as cardiovascular, skeletal muscle and neural networks, which are often overlooked [41]. In living organisms, the estrogen receptors ERα, ERβ and the G protein-coupled estrogen receptor (GPER) play key roles. The coordinated action of these three receptors in the body ensures the effective action of estrogenic substances on target tissues [42]. Estrogen plays an important role in regulating the growth of bone tissue. However, in women, estrogen deficiency during menopause or after bilateral oophorectomy may lead to the loss of cancellous and cortical bone, which in turn can lead to osteoporosis [43–45]. The mechanisms by which estrogen regulates muscle development are unclear, which poses a challenge for further research. In this work, we used the *longissimus dorsi* muscle of small-tailed Han sheep in a sham surgery group (STH) and ovariectomy group (OR-STH) and collected RNA from the *longissimus dorsi* muscle tissue for RNA-seq and molecular biology analysis. We successfully identified 11,297 circRNAs in a comparison between the STH group and the OR-STH group, 118 of which were differentially

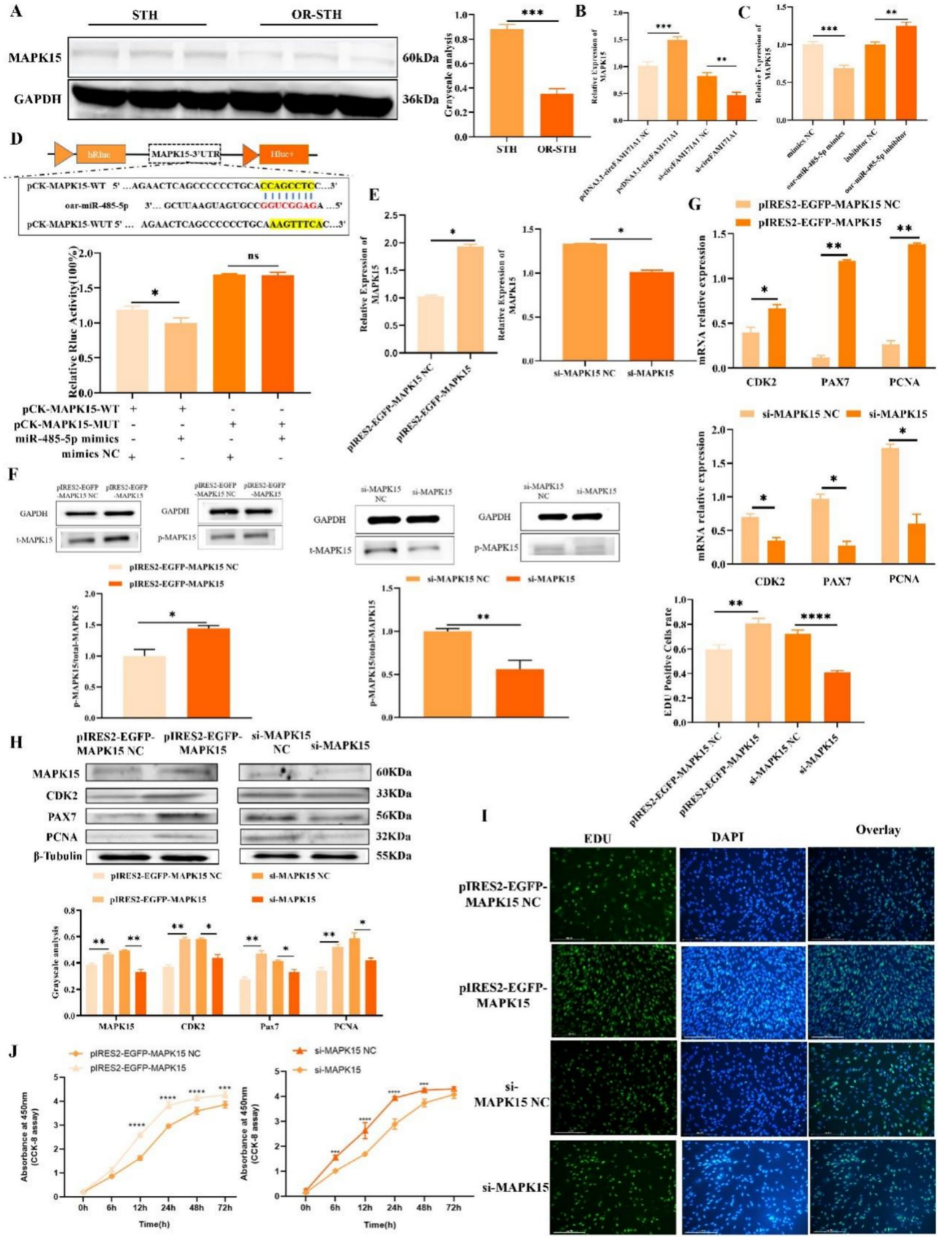
A
STH
OR-STH
MAPK15
GAPDH
60kDa
36kDa
Grayscale analysis
STH
OR-STH
B
Relative Expression of MAPK15
pcDNA3.1-circFAM171A1 NC
pcDNA3.1-circFAM171A1
si-circFAM171A1 NC
si-circFAM171A1
C
Relative Expression of MAPK15
mimics NC
oar-miR-485-5p mimics
inhibitor NC
oar-miR-485-5p inhibitor
D
hRluc
MAPK15-3'UTR
Hluc+
pCK-MAPK15-WT 5' ...AGAACTCAGCCCCCCTGCACCAGCCTCC...3'
oar-miR-485-5p 3'... GCUUAAGUAGUGCCGGUCGGAGA ...5'
pCK-MAPK15-WUT 5' ... AGAACTCAGCCCCCCTGCAAAGTTTCA...3'
Relative Rluc Activity(100%)
ns
pCK-MAPK15-WT
pCK-MAPK15-MUT
miR-485-5p mimics
mimics NC
E
Relative Expression of MAPK15
pIRES2-EGFP-MAPK15 NC
pIRES2-EGFP-MAPK15
si-MAPK15 NC
si-MAPK15
G
pIRES2-EGFP-MAPK15 NC
pIRES2-EGFP-MAPK15
mRNA relative expression
CDK2
PAX7
PCNA
si-MAPK15 NC
si-MAPK15
F
pIRES2-EGFP -MAPK15 NC
pIRES2-EGFP -MAPK15
GAPDH
t-MAPK15
p-MAPK15
p-MAPK15/total-MAPK15
EDU Positive Cells rate
H
pIRES2-EGFP-MAPK15 NC
pIRES2-EGFP-MAPK15
si-MAPK15 NC
si-MAPK15
MAPK15
CDK2
PAX7
PCNA
β-Tubulin
60KDa
33KDa
56KDa
32KDa
55KDa
Grayscale analysis
I
EDU
DAPI
Overlay
pIRES2-EGFP-MAPK15 NC
pIRES2-EGFP-MAPK15
si-MAPK15 NC
si-MAPK15
J
Absorbance at 450nm (CCK-8 assay)
Time(h)
0h
6h
12h
24h
48h
72h

◂**Fig. 8** CircFAM171A1 acts as a sponge for oar-miR-485-5p and impairs the inhibition of MAPK15. **A** The protein level of MAPK15 in muscle tissues of STH compared with OR-STH. **B** Detection of MAPK15 expression in myoblasts after overexpression or inhibition of circFAM171A1. **C** Detection of MAPK15 expression in myoblasts after oar-miR-485-5p overexpression or inhibition. **D** Construction of a putative binding site for oar-miR-485-5p in the 3′-UTR of MAPK15 and a luciferase expression plasmid containing the 3′-UTR of MAPK15. **E** Transfection efficiency of MAPK15 overexpression or interference plasmids. **F** Detection of the phosphorylation level of MAPK15 after overexpression or inhibition of MAPK15. **G** RT−qPCR results showing the expression of *CDK2, Pax7* and *PCNA* after the overexpression or inhibition of MAPK15. **H** Western blotting results of CDK2, Pax7 and PCNA after overexpression or inhibition of MAPK15. **I** An EdU assay revealed that the number of myocytes increased after the overexpression or inhibition of MAPK15 (scale bar: 200 μm). **J** CCK8 assay detection of the proliferation rate of myocytes after overexpression or inhibition of MAPK15. N = 3; the data are expressed as the mean ± SD. ns, not significant, * $P < 0.05$, ** $P < 0.01$, *** $P < 0.001$

expressed. In a follow-up study, the differentially expressed circRNA host genes were analyzed for GO terms and KEGG pathway enrichment. This analysis revealed multiple important pathways involved in muscle growth, development and degradation, such as the AMPK signaling pathway, ECM receptor interactions, the ErbB signaling pathway, ubiquitin-mediated protein hydrolysis and the mTOR signaling pathway. These pathways play key roles in muscle development and are important for muscle growth and functional maintenance [46–49]. As key gene expression regulators, circRNAs play important roles in animal growth and development. Our study revealed that changes in circRNA abundance may be associated with ovariectomy. Further studies on the role of circRNAs in skeletal muscle growth and development will help to elucidate the relevant physiological mechanisms and provide useful references for clinical practice.

In recent years, with the completion of the assembly and annotation of sheep breed genomes, there is now a wealth of reference data for sheep transcriptome analysis. As functionally conserved molecules, circRNAs have been shown to be important for animal development and growth in humans and mice [47–50]. However, few studies on functional circRNAs in sheep have been reported. In this study, circRNA sequencing results revealed that estrogen induced the production of a high abundance of circFAM171A1. We subsequently confirmed this result using in vitro addition of different concentrations of estradiol. In a subsequent study, we used a cell transfection technique to investigate the key role of circFAM171A1 in the proliferation of sheep myoblasts. The experimental results revealed that circFAM171A1 significantly promoted the proliferation of myoblasts. These findings reveal the important role of circFAM171A1 in sheep muscle progression and provide a basis for further research on the function of circRNAs in mammalian muscle biology.

Increasingly, circRNAs have been found to function as miRNA sponges in the cytoplasm. This phenomenon was exemplified by circRNA-UBE2G1, a circRNA found mainly in the cytoplasm. circRNA-UBE2G1 was found to act as a sponge for miR-373 to modulate chondrocyte damage after lipopolysaccharide (LPS) treatment [46]. CircFGFR2 is located in the cytoplasm and can serve as a molecular sponge for miR-133a-5p and miR-29b-1-5p to promote myoblast proliferation and differentiation [47]. In this study, we confirmed that circFAM171A1 was distributed mostly in the cytoplasm through nucleoplasmic separation and fluorescence in situ hybridization (FISH) experiments. Transcriptome integration analysis revealed that circFAM171A1 functions as a ceRNA and mediates the expression of oar-miR-485-5p and MAPK15. Notably, miR-485-5p has been shown to be closely associated with the prevention and treatment of kidney and ovarian cancer [48, 49]. Furthermore, there is substantial evidence that miR-485-5p can function by binding to circRNAs. For example, circRUNX1 elevates SLC38A1 by adsorbing miR-485-5p to promote colorectal cancer cell growth, metastasis, and glutamine metabolism [50]. CircFOXK2 can bind to miR-485-5p and activate PD-L1, thereby accelerating the development of non-small cell lung cancer (NSCLC) [51]. Circ_0008529 modulates high glucose (HG)-induced apoptosis and inflammatory injury in human kidney cells (HK-2) by targeting the miR-485-5p/WNT2B pathway, indicating that Circ_0008529 plays a key role in the development of diabetic nephropathy (DN) [52]. In our study, a dual-luciferase reporter assay confirmed that circFAM171A1 was able to bind oar-miR-485-5p. A functional study further revealed that oar-miR-485-5p could inhibit the proliferation of sheep primary myoblasts. However, overexpression of circFAM171A1 attenuated or even reversed this inhibitory effect. These results indicated that the effect of oar-miR-485-5p is opposite to that of circFAM171A1, suggesting that circFAM171A1 acts as a sponge for oar-miR-485-5p to regulate the proliferation of sheep myoblasts. These findings provide an important basis for further exploration of the functions of circRNAs in biology and medicine.

The optimal working condition of miRNA sponge effect is that circRNA and miRNA concentrations are equivalent. However, the effectiveness of miRNA sponge effect is not entirely dependent on the change multiple of circRNA expression, but on the relative concentration and affinity between circRNA and miRNA. Even if the expression of circRNA does not change much, if the concentration of miRNA is also relatively low, the sponge effect may still occur. To more accurately evaluate the interaction between circFAM171A1 and oar-miR-485-5p, we validated this interaction through RNA pull-down experiments. This experimental approach was able to provide direct evidence of whether binding between circRNA and miRNA occurs, and the strength of this binding. In summary, although

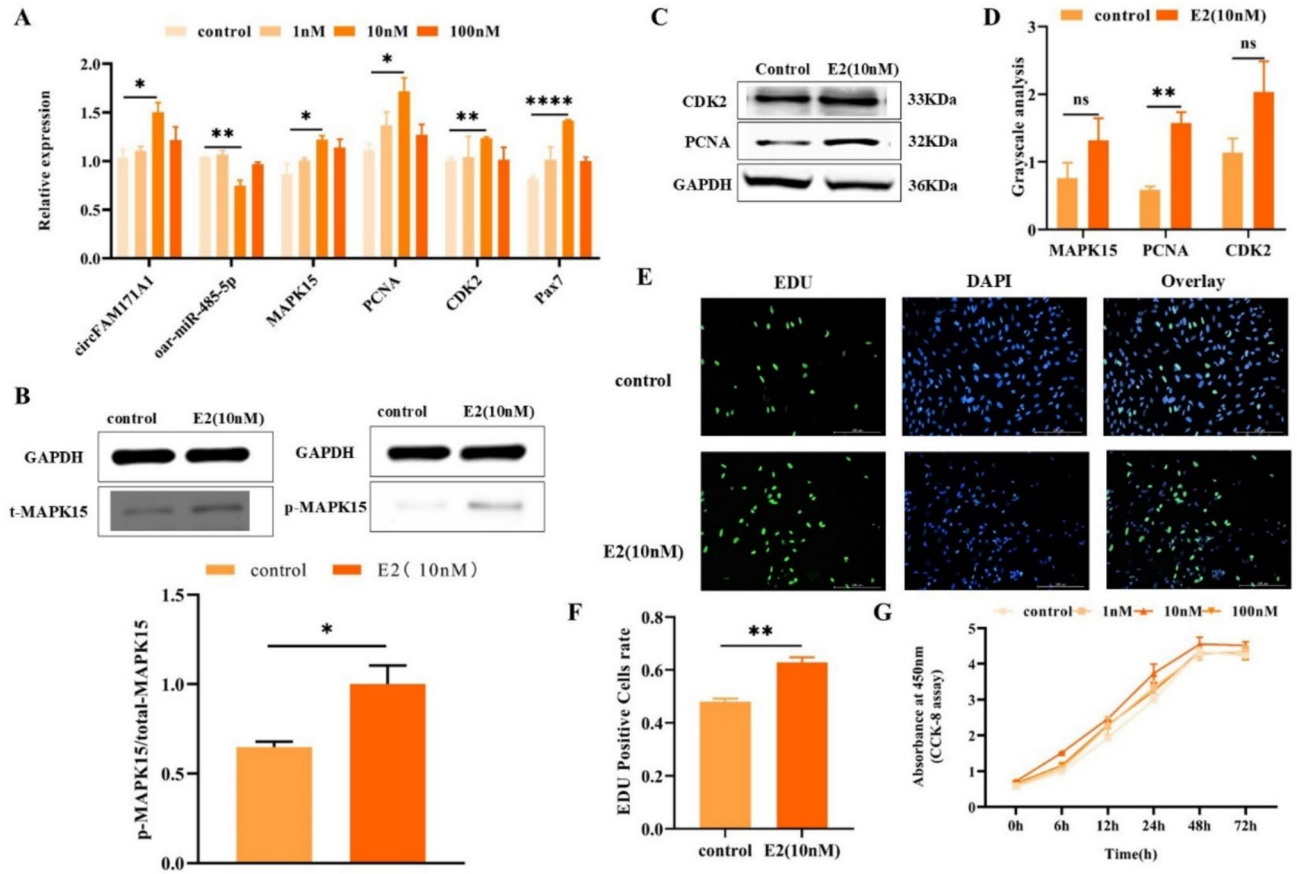

Fig. 9 Estradiol (E_2) affects the proliferation of sheep myoblasts via the circFAM171A1/oar-miR-485-5p/MAPK15 pathway. **A** Expression of oar-miR-485-5p, *MAPK15, CDK2* and *PCNA* in sheep myoblasts after the addition of estradiol. β-actin was used as an internal control. **B** The phosphorylation level of MAPK15 was also increased by the addition of 10 nM estradiol. **C**, **D** Protein expression and gray value analysis of MAPK15, PCNA and CDK2 in sheep myoblasts after the addition of estradiol. β-Tubulin was used as an internal control. **E**, **F** EdU assay analysis of the proliferation of sheep myoblasts supplemented with estradiol. **G** CCK-8 assay analysis of the proliferation of sheep myoblasts supplemented with estradiol. N = 3; the data are expressed as the mean ± SD. ns, not significant, * $P < 0.05$, ** $P < 0.01$, *** $P < 0.001$

circFAM171A1 expression changes little, it does not rule out the possibility of miRNA sponge effect. We took into account the concentration, affinity and biological background of circRNA and miRNA, and confirmed the role of circFAM171A1 as an oar-miR-485-5p sponge through experimental verification. This interaction may have important effects on the regulation of miRNA activity and gene expression in cells, which is worthy of further study and exploration.

The discovery that MAPK15, ERK8 and MAPK7 (ERK7) are atypical members of the MAP kinase family has provided a new perspective on the study of the MAP kinase family, a group of serine/threonine kinases that are widely found in eukaryotes and play key roles in cell growth, differentiation, apoptosis and other biological processes [53]. MAPK8 and MAPK11 are also important members of the MAP kinase family [21]. circACTA1 can act as a miR199a-5p and miR-433 sponge, thereby eliminating the inhibitory effect on the target genes MAP3K11 and MAPK8. circACTA1 further affects the biological behavior of bovine primary myoblasts by activating the MAP3K11/MAP2K7/JNK signaling pathway. During cell proliferation, apoptosis and differentiation, circACTA1 plays an important regulatory role [21]. Moreover, miR-138 prevents anoxia-induced apoptosis in cardiomyocytes through the MAP3K11/JNK/c-Jun pathway [54]. Recent studies have shown that MAPK15 affects BCR-ABL 1-induced phagocytosis and modulates cancer gene-dependent cell proliferation and neighboring tumor formation [55]. Building on these findings, we hypothesized that circFAM171A1 modulates cell growth through the oar-miR-485-5p/MAPK15 signaling pathway. In this study, overexpression of circFAM171A1 significantly increased the expression of MAPK15. However, interference with circFAM171A1 had the opposite effect. Transfection of mimics of oar-miR-485-5p significantly decreased MAPK15 expression, but treatment with inhibitors of oar-miR-485-5p had the opposite effect. These results suggest

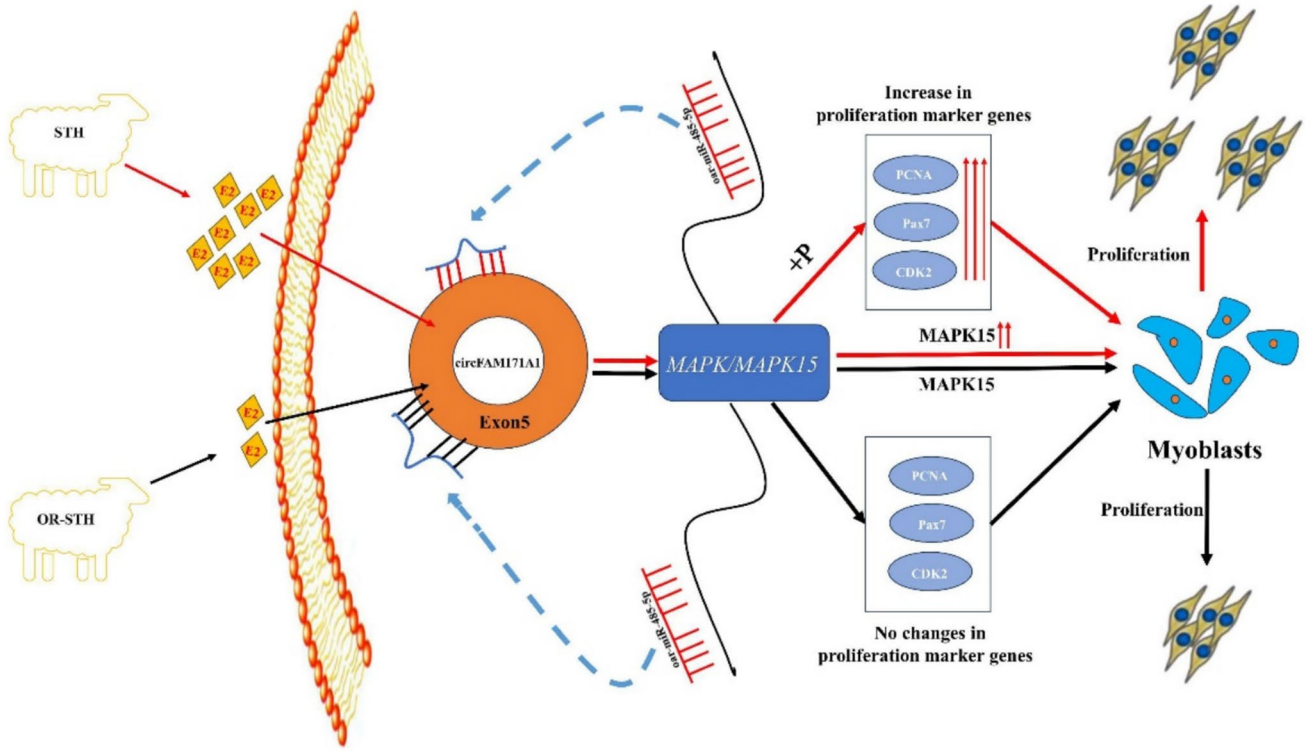

Fig. 10 Schematic of estrogen regulation of sheep myoblast proliferation through the circFAM171A1/oar-miR-485-5p/MAPK15 pathway

that circFAM171A1 can regulate sheep myoblast proliferation via the oar-miR-485-5p/MAPK1 pathway.

Estrogen deficiency has been found to induce hormonal endocrine and metaphorical disruption in women after menopause, resulting in osteoporosis, metabolic syndrome, and loss of muscle force and mass [56]. Studies have shown that estrogen therapy reduces hepatic lipoatrophy by increasing liver aquaporin 7 (AQP7) secretion in an ovariectomized (OR) mouse phantom and a steatosis cell model [57]. Seko et al. confirmed that estrogen has a modulatory role in muscle growth and rejuvenation in young adult female mice via ERβ in bone muscle-specific stem cells [58]. We found that the addition of estradiol to sheep myoblasts promoted their proliferation and that the expression level of oar-miR-485-5p decreased, whereas that of MAPK15 increased. These results suggest that the addition of appropriate levels of estrogen stimulates the growth and proliferation of sheep myoblasts through the circFAM171A1/oar-miR-485-5p/MAPK15 pathway.

Conclusion

In this study, we found that estrogen induced circFAM171A1 expression in sheep myoblasts. Transcriptome integration analysis revealed that circFAM171A1 can act as a ceRNA to regulate the expression of oar-miR-485-5p and MAPK15 in sheep myoblasts. In vitro addition of estrogen promoted myoblast proliferation through the circFAM171A1/oar-miR-485-5p/MAPK15 pathway. These findings offer new perspectives for further knowledge of estrogen regulation of myoblast proliferation in female animals and provide insights into the molecular processes by which estrogen affects muscle uptake and growth.

Supplementary Information The online version contains supplementary material available at https://doi.org/10.1007/s00018-025-05639-3.

Acknowledgements The author wishes to thank their collaborators for their technical and academic support.

Author contributions Conceptualization: Runqing Chi, Yufang Liu, Peng Wang. Formal analysis: Runqing Chi, Peng Wang. Funding acquisition: Mingxing Chu. Investigation: Runqing Chi, Yufang Liu, Peng Wang. Project administration: Yufang Liu, Ran Di, Mingxing Chu. Resources: Peng Wang,Fan Yang, Xiangyu Wang. Validation: Runqing Chi, Fan Yang. Writing—original draft: Runqing Chi, Yufang Liu. Writing—review & editing: Runqing Chi, Yufang Liu, Peng Wang, Fan Yang, Xiangyu Wang, Xiaoyun He, Ran Di, Mingxing Chu.

Funding Anhui Provincial Key Laboratory of Livestock and Poultry Product Safety Engineering, XM2404, Yufang Liu, National Natural Science Foundation of China, 32172704, Mingxing Chu, Agricultural Science and Technology Innovation Program of China, CAAS-ZDRW202106, Mingxing Chu, ASTIP-IAS13, Mingxing Chu, China Agriculture Research System of MOF and MARA,CARS-38, Mingxing

Chu, Postdoctoral Fellowship Program of CPSF, GZC20233053, Yufang Liu.

Availability of data and material All the data supporting the findings of this study are available within the manuscript. The data will be made available upon reasonable request. The RNA-seq data accession number for this paper is GEO: GSE288804.

Declaration

Conflict of interests The authors declare that they have no conflicts of interest.

Ethical approval and consent to participate The study was approved by the IAS-CAAS Animal Ethics Committee under approval number IAS2019-63. In strict compliance with relevant regulations, we are committed to promoting animal science research to contribute to the development of agriculture in China.

Consent for publication All the authors involved in this manuscript give consent for publication.

References

1. Collins BC, Laakkonen EK, Lowe DA (2019) Aging of the musculoskeletal system: how the loss of estrogen impacts muscle strength. Bone 123:137–144
2. Vasconsuelo A, Milanesi L, Boland R (2010) Participation of HSP27 in the antiapoptotic action of 17beta-estradiol in skeletal muscle cells. Cell Stress Chaperones 15(2):183–192
3. Boland R, Vasconsuelo A, Milanesi L, Ronda AC, de Boland AR (2008) 17beta-estradiol signaling in skeletal muscle cells and its relationship to apoptosis. Steroids 73(9–10):859–863
4. La Colla A, Boland R, Vasconsuelo A (2015) 17β-Estradiol abrogates apoptosis inhibiting PKCδ, JNK, and p66Shc activation in C2C12 cells. J Cell Biochem 116(7):1454–1465
5. La Colla A, Vasconsuelo A, Boland R (2013) Estradiol exerts antiapoptotic effects in skeletal myoblasts via mitochondrial PTP and MnSOD. J Endocrinol 216(3):331–341
6. La Colla A, Vasconsuelo A, Milanesi L, Pronsato L (2017) 17β-estradiol protects skeletal myoblasts from apoptosis through p53, Bcl-2, and FoxO families. J Cell Biochem 118(1):104–115
7. Ronda AC, Vasconsuelo A, Boland R (2010) Extracellular-regulated kinase and p38 mitogen-activated protein kinases are involved in the antiapoptotic action of 17beta-estradiol in skeletal muscle cells. J Endocrinol 206(2):235–246
8. Ronda AC, Vasconsuelo A, Boland R (2013) 17β-estradiol protects mitochondrial functions through extracellular-signal-regulated kinase in C2C12 muscle cells. Cell Physiol Biochem 32(4):1011–1023
9. Paroo Z, Dipchand ES, Noble EG (2002) Estrogen attenuates postexercise HSP70 expression in skeletal muscle. Am J Physiol Cell Physiol 282(2):C245-251
10. Paroo Z, Tiidus PM, Noble EG (1999) Estrogen attenuates HSP 72 expression in acutely exercised male rodents. Eur J Appl Physiol 80(3):180–184
11. Bombardier E, Vigna C, Bloemberg D, Quadrilatero J, Tiidus PM, Tupling AR (2013) The role of estrogen receptor-α in estrogen-mediated regulation of basal and exercise-induced Hsp70 and Hsp27 expression in rat soleus. Can J Physiol Pharmacol 91(10):823–829
12. Bombardier E, Vigna C, Iqbal S, Tiidus PM, Tupling AR (2009) Effects of ovarian sex hormones and downhill running on fiber-type-specific HSP70 expression in rat soleus. J Appl Physiol (Bethesda, Md: 1958) 106(6):2009–2015
13. Wang H, Alencar A, Lin M, Sun X, Sudo RT, Zapata-Sudo G, Lowe DA, Groban L (2016) Activation of GPR30 improves exercise capacity and skeletal muscle strength in senescent female Fischer344 × Brown Norway rats. Biochem Biophys Res Commun 475(1):81–86
14. Karvinen S, Juppi HK, Le G, Cabelka CA, Mader TL, Lowe DA, Laakkonen EK (2021) Estradiol deficiency and skeletal muscle apoptosis: possible contribution of microRNAs. Exp Gerontol 147:111267
15. Wang L, Yi J, Lu LY, Zhang YY, Wang L, Hu GS, Liu YC, Ding JC, Shen HF, Zhao FQ et al (2021) Estrogen-induced circRNA, circPGR, functions as a ceRNA to promote estrogen receptor-positive breast cancer cell growth by regulating cell cycle-related genes. Theranostics 11(4):1732–1752
16. Jeck WR, Sharpless NE (2014) Detecting and characterizing circular RNAs. Nat Biotechnol 32(5):453–461
17. Li Z, Huang C, Bao C, Chen L, Lin M, Wang X, Zhong G, Yu B, Hu W, Dai L et al (2015) Exon-intron circular RNAs regulate transcription in the nucleus. Nat Struct Mol Biol 22(3):256–264
18. Ashwal-Fluss R, Meyer M, Pamudurti NR, Ivanov A, Bartok O, Hanan M, Evantal N, Memczak S, Rajewsky N, Kadener S (2014) circRNA biogenesis competes with pre-mRNA splicing. Mol Cell 56(1):55–66
19. Starke S, Jost I, Rossbach O, Schneider T, Schreiner S, Hung LH, Bindereif A (2015) Exon circularization requires canonical splice signals. Cell Rep 10(1):103–111
20. Chen W, Schuman E (2016) Circular RNAs in brain and other tissues: a functional enigma. Trends Neurosci 39(9):597–604
21. Qi A, Ru W, Yang H, Yang Y, Tang J, Yang S, Lan X, Lei C, Sun X, Chen H (2022) Circular RNA ACTA1 Acts as a Sponge for miR-199a-5p and miR-433 to regulate bovine myoblast development through the MAP3K11/MAP2K7/JNK Pathway. J Agric Food Chem 70(10):3357–3373
22. Chen B, Yu J, Guo L, Byers MS, Wang Z, Chen X, Xu H, Nie Q (2019) Circular RNA circhipk3 promotes the proliferation and differentiation of chicken myoblast cells by sponging miR-30a-3p. Cells 8(2):177
23. Zhu M, Lian C, Chen G, Zou P, Qin BG (2021) CircRNA FUT10 regulates the regenerative potential of aged skeletal muscle stem cells by targeting HOXA9. Aging 13(13):17428–17441
24. Yang Z, Song C, Jiang R, Huang Y, Lan X, Lei C, Qi X, Zhang C, Huang B, Chen H (2022) CircNDST1 regulates bovine myoblasts proliferation and differentiation via the miR-411a/Smad4 Axis. J Agric Food Chem 70(32):10044–10057
25. Du WW, Yang W, Liu E, Yang Z, Dhaliwal P, Yang BB (2016) Foxo3 circular RNA retards cell cycle progression via forming

ternary complexes with p21 and CDK2. Nucleic Acids Res 44(6):2846–2858
26. Legnini I, Di Timoteo G, Rossi F, Morlando M, Briganti F, Sthandier O, Fatica A, Santini T, Andronache A, Wade M et al (2017) Circ-ZNF609 is a circular RNA that can be translated and functions in myogenesis. Mol Cell 66(1):22-37.e29
27. Wei X, Li H, Yang J, Hao D, Dong D, Huang Y, Lan X, Plath M, Lei C, Lin F et al (2017) Circular RNA profiling reveals an abundant circLMO7 that regulates myoblasts differentiation and survival by sponging miR-378a-3p. Cell Death Dis 8(10):e3153
28. Sun J, Xie M, Huang Z, Li H, Chen T, Sun R, Wang J, Xi Q, Wu T, Zhang Y (2017) Integrated analysis of non-coding RNA and mRNA expression profiles of 2 pig breeds differing in muscle traits. J Anim Sci 95(3):1092–1103
29. Yue B, Wang J, Song C, Wu J, Cao X, Huang Y, Lan X, Lei C, Huang B, Chen H (2019) Biogenesis and ceRNA role of circular RNAs in skeletal muscle myogenesis. Int J Biochem Cell Biol 117:105621
30. Chen MM, Zhao YP, Zhao Y, Deng SL, Yu K (2021) Regulation of myostatin on the growth and development of skeletal muscle. Front Cell Develop Biol 9:785712
31. Buckingham M, Relaix F (2015) PAX3 and PAX7 as upstream regulators of myogenesis. Semin Cell Dev Biol 44:115–125
32. Megeney LA, Rudnicki MA (1995) Determination versus differentiation and the MyoD family of transcription factors. Biochem Cell Biol 73(9–10):723–732
33. Daubas P, Buckingham ME (2013) Direct molecular regulation of the myogenic determination gene Myf5 by Pax3, with modulation by Six1/4 factors, is exemplified by the -111 kb-Myf5 enhancer. Dev Biol 376(2):236–244
34. Kassar-Duchossoy L, Gayraud-Morel B, Gomès D, Rocancourt D, Buckingham M, Shinin V, Tajbakhsh S (2004) Mrf4 determines skeletal muscle identity in Myf5: Myod double-mutant mice. Nature 431(7007):466–471
35. Fan CM, Li L, Rozo ME, Lepper C (2012) Making skeletal muscle from progenitor and stem cells: development versus regeneration. Wiley Interdiscip Rev Dev Biol 1(3):315–327
36. Yin H, Price F, Rudnicki MA (2013) Satellite cells and the muscle stem cell niche. Physiol Rev 93(1):23–67
37. Xie C, Mao X, Huang J, Ding Y, Wu J, Dong S, Kong L, Gao G, Li CY, Wei L (2011) KOBAS 2.0: a web server for annotation and identification of enriched pathways and diseases. Nucleic acids research, 39(Web Server issue): W316–322.
38. Wang X, Cao X, Dong D, Shen X, Cheng J, Jiang R, Yang Z, Peng S, Huang Y, Lan X et al (2019) Circular RNA TTN Acts As a miR-432 sponge to facilitate proliferation and differentiation of myoblasts via the IGF2/PI3K/AKT signaling pathway. Mol Ther Nucleic Acids 18:966–980
39. Xiong Y, Zhang J, Song C (2019) CircRNA ZNF609 functions as a competitive endogenous RNA to regulate FOXP4 expression by sponging miR-138-5p in renal carcinoma. J Cell Physiol 234(7):10646–10654
40. Kristensen LS, Andersen MS, Stagsted LVW, Ebbesen KK, Hansen TB, Kjems J (2019) The biogenesis, biology and characterization of circular RNAs. Nat Rev Genet 20(11):675–691
41. Mauvais-Jarvis F, Clegg DJ, Hevener AL (2013) The role of estrogens in control of energy balance and glucose homeostasis. Endocr Rev 34(3):309–338
42. Eyster KM (2016) The estrogen receptors: an overview from different perspectives. Methods Mol Biol (Clifton, NJ) 1366:1–10
43. Pöllänen E, Sipilä S, Alen M, Ronkainen PH, Ankarberg-Lindgren C, Puolakka J, Suominen H, Hämäläinen E, Turpeinen U, Konttinen YT et al (2011) Differential influence of peripheral and systemic sex steroids on skeletal muscle quality in pre- and postmenopausal women. Aging Cell 10(4):650–660
44. Gillies GE, McArthur S (2010) Estrogen actions in the brain and the basis for differential action in men and women: a case for sex-specific medicines. Pharmacol Rev 62(2):155–198
45. Dumont NA, Bentzinger CF, Sincennes MC, Rudnicki MA (2015) Satellite cells and skeletal muscle regeneration. Compr Physiol 5(3):1027–1059
46. Chen G, Liu T, Yu B, Wang B, Peng Q (2020) CircRNA-UBE2G1 regulates LPS-induced osteoarthritis through miR-373/HIF-1a axis. Cell Cycle (Georgetown, Tex) 19(13):1696–1705
47. Chen X, Ouyang H, Wang Z, Chen B, Nie Q (2018) A Novel Circular RNA generated by FGFR2 gene promotes myoblast proliferation and differentiation by sponging miR-133a-5p and miR-29b-1–5p. Cells 7(11):199
48. Liu H, Hu G, Wang Z, Liu Q, Zhang J, Chen Y, Huang Y, Xue W, Xu Y, Zhai W (2020) circPTCH1 promotes invasion and metastasis in renal cell carcinoma via regulating miR-485-5p/MMP14 axis. Theranostics 10(23):10791–10807
49. Wang W, Yu S, Li W, Hu H, Zou G (2022) Silencing of lncRNA SNHG17 inhibits the tumorigenesis of epithelial ovarian cancer through regulation of miR-485-5p/AKT1 axis. Biochem Biophys Res Commun 637:117–126
50. Yu J, Chen X, Li J, Wang F (2021) CircRUNX1 functions as an oncogene in colorectal cancer by regulating circRUNX1/miR-485-5p/SLC38A1 axis. Eur J Clin Invest 51(7):e13540
51. Zhang N, Fan J, Deng Z (2022) CircFOXK2 enhances tumorigenesis and immune evasion in non-small cell lung cancer by miR-485-5p/PD-L1 axis. Anticancer Drugs 33(5):437–447
52. Wang W, Lu H (2022) High glucose-induced human kidney cell apoptosis and inflammatory injury are alleviated by Circ_0008529 Knockdown via Circ_0008529-mediated miR-485-5p/WNT2B signaling. Appl Biochem Biotechnol 194(12):6287–6301
53. Franci L, Tubita A, Bertolino FM, Palma A, Cannino G, Settembre C, Rasola A, Rovida E, Chiariello M (2022) MAPK15 protects from oxidative stress-dependent cellular senescence by inducing the mitophagic process. Aging Cell 21(7):e13620
54. He S, Liu P, Jian Z, Li J, Zhu Y, Feng Z, Xiao Y (2013) miR-138 protects cardiomyocytes from hypoxia-induced apoptosis via MLK3/JNK/c-jun pathway. Biochem Biophys Res Commun 441(4):763–769
55. Colecchia D, Rossi M, Sasdelli F, Sanzone S, Strambi A, Chiariello M (2015) MAPK15 mediates BCR-ABL1-induced autophagy and regulates oncogene-dependent cell proliferation and tumor formation. Autophagy 11(10):1790–1802
56. Ikeda K, Horie-Inoue K, Inoue S (2019) Functions of estrogen and estrogen receptor signaling on skeletal muscle. J Steroid Biochem Mol Biol 191:105375
57. Fu X, Xing L, Xu W, Shu J (2016) Treatment with estrogen protects against ovariectomy-induced hepatic steatosis by increasing AQP7 expression. Mol Med Rep 14(1):425–431
58. Seko D, Fujita R, Kitajima Y, Nakamura K, Imai Y, Ono Y (2020) Estrogen receptor β controls muscle growth and regeneration in young female mice. Stem Cell Rep 15(3):577–586